
©ISTOCKPHOTO.COM/GREYFEBRUARY

# Nonprecious Electrocatalysts for Li–Air and Zn–Air Batteries

## Fundamentals and recent advances.

TONGWEN YU, JING FU, RUI CAI, AIPING YU, AND ZHONGWEI CHEN

*Digital Object Identifier 10.1109/MNANO.2017.2710380*
*Date of publication: 10 July 2017*

OVER THEIR 150-YEAR HISTORY, new twists on metal–air batteries have continued to emerge up to the present day. In this article, we present the fundamentals and recent advances in nonprecious electrocatalysts for metal–air batteries. The catalysts for oxygen reduction reaction (ORR) and oxygen evolution reaction (OER) in lithium (Li)–air and zinc (Zn)–air batteries, including transition-metal oxides, inorganic–organic hybrid materials, and metal-free materials, are summarized. Both aqueous and nonaqueous systems are also considered. We briefly introduce the mechanism and challenges of oxygen electrochemistry and provide a perspective on the design and development of nonprecious electrocatalysts.

## OVERVIEW OF METAL–AIR BATTERIES

The increasing importance of energy storage in the 21st century will bring about a revolution in energy-storage technologies. A few technologies, such as wind, solar, pumped hydroelectric, compressed air, flywheels, rechargeable batteries, and molten salt-based thermal storage, will be vital to meet the growth in energy demand and achieve the decarbonization transition [1]. Of these technologies, batteries are perhaps the most versatile. Their diverse applications range from portable electronics to emerging electric vehicles. Among batteries, metal–air batteries have attracted much attention because of their extremely high specific energy density compared to that of other rechargeable batteries [2], [3] and the interesting open structure of air electrodes with gaseous active materials [4].

Compared to traditional batteries, the most significant characteristic of metal–air batteries in the components is the air-breathing electrode, which

Metal–air batteries have attracted much attention because of their extremely high specific energy density compared to that of other rechargeable batteries.

admits the supply of the cathode active material (oxygen) continuously from an external air source. The metal–air battery is composed of a metal electrode that can be Li, Zn, aluminum (Al), sodium (Na), magnesium (Mg), calcium (Ca), and iron (Fe) [5]; an air electrode; and a separator soaked in metal-ion conducting electrolyte [6], [7]. Electricity is generated through redox (reduction and oxidation) processes between metal and oxygen. During discharge, metal cations react with dissolved oxygen and electrons to form a metal-oxide or metal-hydroxide discharge product. During charge, the discharge phase is decomposed back to oxygen and dissolved metal cations [8]. Metal–air batteries have notably higher theoretical energy densities than traditional batteries, such as lead-acid, nickel–cadmium (Ni-Cd), and Li-ion batteries (LIBs) [9], and some are even close to the value of gasoline, as shown in Figure 1.

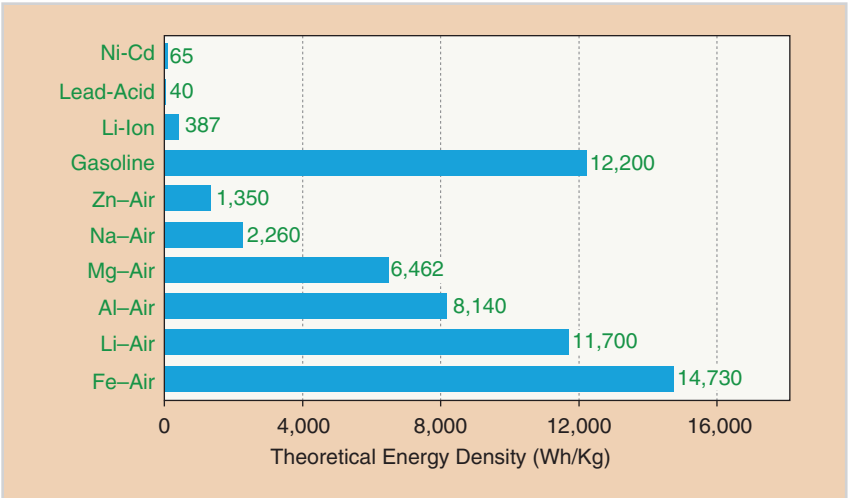


**FIGURE 1** The theoretical energy densities of rechargeable batteries compared to gasoline.

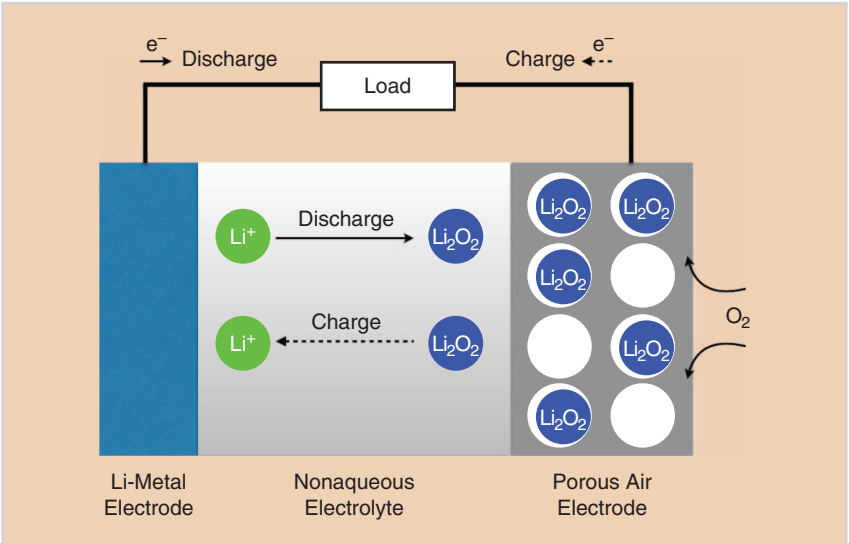


**FIGURE 2** The typical discharge and charge processes in nonaqueous electrolyte-based Li–air batteries.

In the metal–air family, Li–air and Zn–air batteries are emerging as promising candidates for commercial technologies because Li is the most electronegative and lightest metal, while Zn is highly abundant, low cost, and environmentally compatible [3], [10]. As a result, they are the focus of this article.

## *LI–AIR BATTERIES*

Modern rechargeable Li–air batteries with nonaqueous electrolytes were invented in 1996 [11]. They were given a great deal of attention by Ogasawara et al. in 2006 because their performance of tens of charge/recharge cycles was promising for practical applications [12]. Furthermore, Li–air could release an extremely high theoretical specific energy of ~11,700 Wh/kg (based on the mass of Li alone, and the electrode oxygen is not stored in the system), nearly equivalent to that of gasoline [2], [13] (Figure 1). For nonaqueous Li–air batteries, upon discharge, the Li-metal anode is oxidized, releasing $Li^+$ and electrons. Specifically, oxygen is thought to react with $Li^+$ present in the electrolyte to form Li oxides (typically $Li_2O_2$) [14], [15]. On charge, the chemical reaction reverses to evolve oxygen gas [6], [13]. However, the previously formed discharged products must be removed, as they may clog the pores of the air electrode after a few discharge/charge cycles, degrading the battery performance [16], [17]. The reaction processes are $2Li^+ + O_2 + 2e^- \Leftrightarrow Li_2O_2$, as shown in Figure 2. That redox mechanism is inherently different from the intercalation/deintercalation reaction mechanism in LIBs.

The Li–air batteries can be categorized into four architectures based on the type of electrolytes: nonaqueous electrolyte, aqueous electrolyte, hybrid aqueous/nonaqueous electrolytes, and solid-state electrolyte [18]. Their configurations are shown in Figure 3 [3]. For nonaqueous Li–air batteries, similar to LIBs, carbonate-based electrolytes, such as propylene carbonate, and other carbonate mixtures have been widely used due to a wide electrochemical window, low volatility, and wide liquid temperature range from –50 to 240 °C [2], [19]. However, carbonate-based electrolytes are susceptible to nucleophilic attack by the superoxide radical formed upon discharge, thus having limited anodic oxidation stability [20]–[25]. Other organic solvents, such as ethers [17], acetonitrile [26], [27], dimethyl sulfoxide [28], and ionic liquids [29]–[34], also were investigated. Furthermore, nonaqueous electrolytes could determine the fundamental electrochemistry to some degree, e.g., the discharge/charge reactions, parasitic side reactions, and battery performance.

Compared to nonaqueous electrolytes, the aqueous electrolytes do not limit the battery performance and avoid the unsafe problem of battery burning [35]. However, the main disadvantage of aqueous electrolytes is the relatively low decomposition voltage (its theoretical potential is only 1.23 V), which leads to a certain rate of self-discharge above that potential [4]. In addition, an Li electrode usually reacts excessively with water and corrodes. Thus, it is necessary to set an artificial solid electrolytic interface (SEI), typically Li-ion-conducting ceramic or glass, such as Li superionic conductor (LiSICON)-type [e.g., $LiM_2(PO_4)_3$] or Na superionic conductor (NaSICON)-type materials (e.g., $Li_{1+x+y}Al_xTi_{2-x}Si_yP_{3-y}O_{12}$) [36]–[45] to encase the Li electrode. However, the thickness of these membranes usually reaches a few hundred micrometers, and it causes a large $iR$ voltage drop at higher currents and therefore limits power density. Furthermore, the brittle nature of SEI may result in barrier cracks upon charge–discharge cycling and lead to parasitic reactions at the electrode surface [13]. Thus, thinner and mechanically stable protective layers for preventing the corrosion of Li metal by water remain a great challenge in aqueous systems [46]–[48].

Hybrid aqueous/nonaqueous electrolyte-based Li–air batteries merge benefits with aqueous electrolyte-based batteries to alleviate the problems

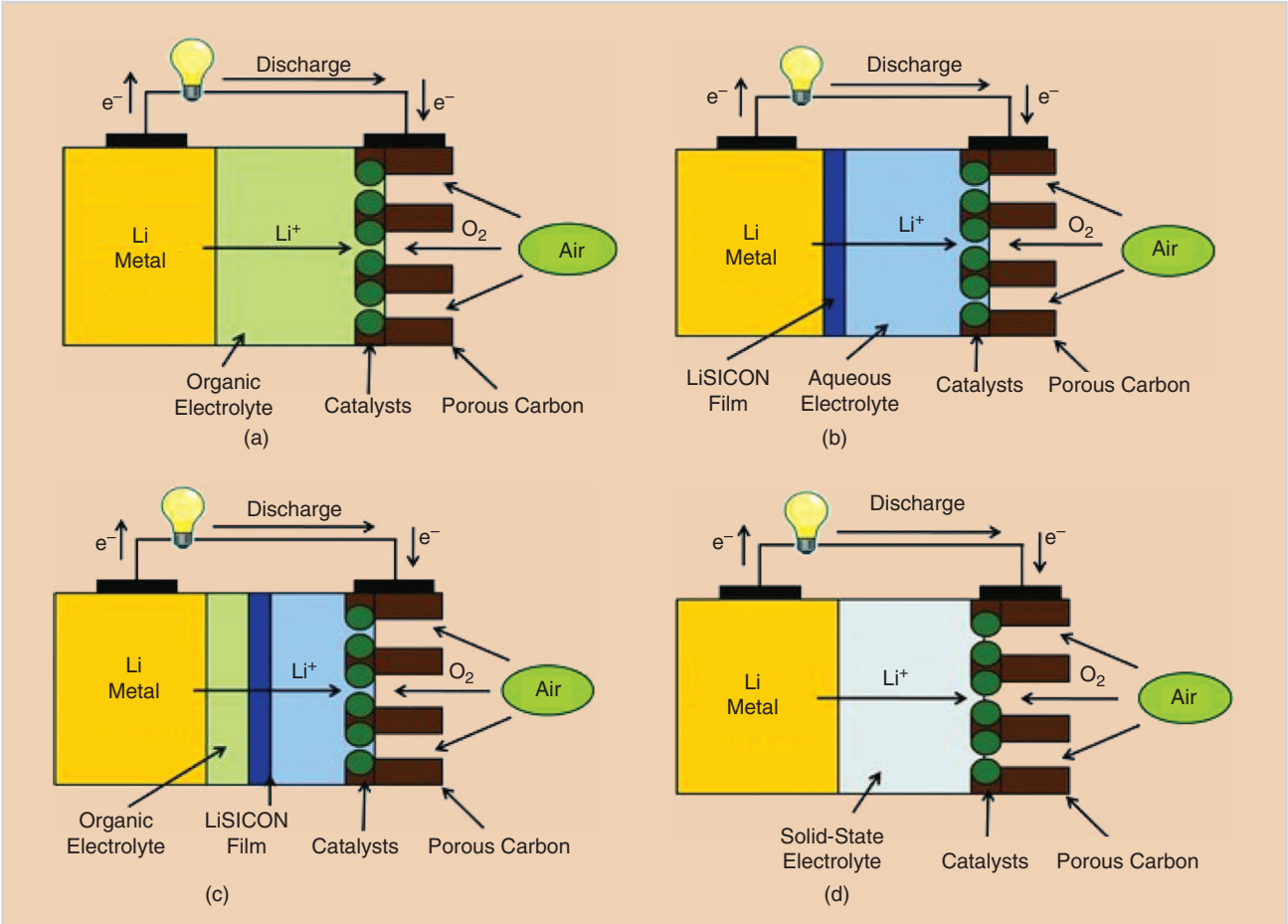


**FIGURE 3** The schematic cell configurations for the four types of Li–air batteries: (a) nonaqueous, (b) aqueous, (c) hybrid, and (d) solid-state electrolyte. (Figure courtesy of Wiley-VCH Verlag GmbH and Co. KGaA, Weinheim.)

of nonaqueous systems, e.g., the detrimental side reactions at metal electrodes [49]–[51]. The two types of electrolytes are separated by an $Li^+$-conducting membrane (LiSICON-type and NaSICON-type). But its low $Li^+$ conductivity and instability in both strong acidic and strong basic solutions are currently the bottlenecks for hybrid and aqueous Li–air batteries [36], [52]. Another challenge is the formation of Li dendrite that occurs upon cycling, as it further reduces and damages the NaSICON-type materials by contacting Li [52], [53].

Solid-state electrolytes involve inorganic $Li^+$ ion conductors [e.g., $Li_{1+x}Al_xGe_{2-x}(PO_4)_3$] and solid organic electrolytes [e.g., poly(ethylene oxide)-LiX (X, anion) polymer composite] [54]. They have wide electrochemical windows, and they are relatively stable compared to the organic liquid electrolyte. Furthermore, the solid-state electrolyte membrane in the system could prevent the Li electrode from reacting with $H_2O$ and $CO_2$ in air due to its nonpermeability of humidity and $CO_2$. However, the interfacial charge-transfer process is the major resistance [54].

## ZN–AIR BATTERIES

Zn–air batteries, with the advantages of low cost, excellent safety, environmentally friendly properties, and flexibility and stretchability, have received much attention [55], [56]. Their theoretical energy density is 1,350 Wh/kg, approximately three times higher than that of the current LIBs [55]–[57].

In a Zn–air battery, pure Zn metal acts as the active electrode material, and the most widely used electrolyte is alkaline media, such as potassium hydroxide (typically 30 wt %) [58]–[62] and NaOH [63]–[65]. In the alkaline electrolyte, the following anode reactions (1), (2), (3) occur upon discharge:

$$Zn \rightarrow Zn^{2+} + 2e^-, \quad (1)$$

$$Zn^{2+} + 4OH^- \rightarrow Zn(OH)_4^{2-}, \quad (2)$$

$$Zn(OH)_4^{2-} \rightarrow ZnO + H_2O + 2OH^-. \quad (3)$$

Solid powders (ZnO) act as an insulater and lead to the formation of dendrites in the charge–discharge cycling process, thus degrading the performance [3] [66], [67] and even making the battery difficult to recharge [68]. Therefore, the issue of Zn dissolution is the principal limitation for rechargeable Zn electrodes. Experimental evidence shows that additives, such as potassium fluoride and surfactants (e.g., tetra-alkyl ammonium hydroxides), could significantly inhibit the growth of Zn dendrite [69]–[73].

Studying how to improve the electrochemical performance of a Zn anode is a good strategy of improving the battery performance. The major effects carried out are alloying or coating the Zn active materials. One approach is to increase the surface area of Zn particles, such as $Zn/MnO_2$ and Zn/NiOOH [69], [74]. However, more effects should be focused on understanding the chemistry and behavior of the zincate ions in alkaline electrolyte [75]–[79]. Some research suggests that the pH of the electrolyte greatly affects the diversity of possible zincate ions. $Zn(OH)_4^{2-}$ is the principal species in the strong alkaline solution with pH ≥ 13. With the value of pH between 9.3 and 12.3, the intermediate species $Zn(OH)_y^{2-y}$ (y varies from 0 to 4) is formed [80], [81]. A simple Pourbaix diagram is shown in Figure 4 [82].

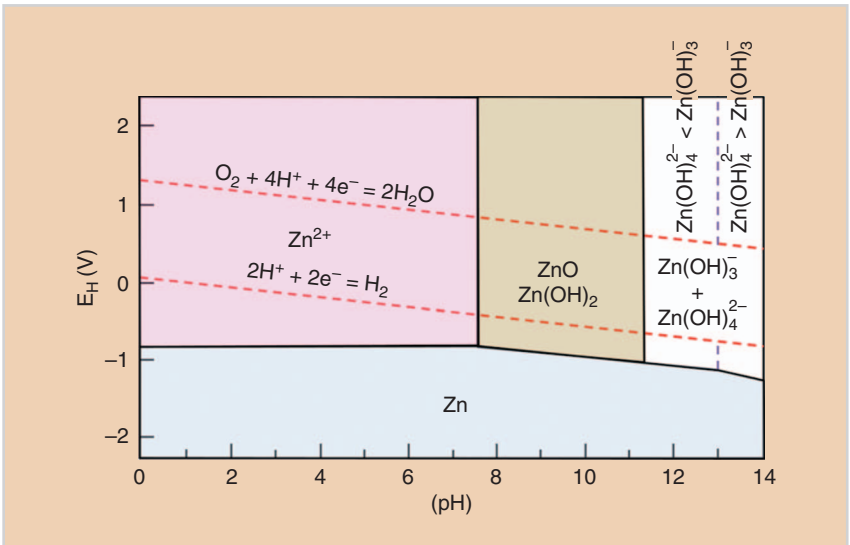


**FIGURE 4** A Pourbaix diagram of Zn in alkaline electrolyte at 25 °C. (Figure courtesy of Wiley.)

Flexible batteries in portable electronic devices are becoming favorites of the modern market. However, typical liquid electrolytes are not suitable for flexible Zn–air batteries due to issues of evaporation and leakage [57]. The solid-state electrolyte, e.g., gelatin-based gel-polymer electrolyte [57] or hydrogel-polymer electrolyte [55] with conformable shape, could be utilized in flexible and wearable devices. Specifically, a porous-gelled poly(vinyl) alcohol (PVA) polymer electrolyte membrane and electrode with high flexiblity could be used to fabricate a portable and wearable Zn–air battery (Figure 5) [56]. Furthermore, a nanoporous alkaline-exchange electrolyte membrane has been used as the solid-state electrolyte for rechargeable Zn–air batteries [83]. The performance of the existing Li–air and Zn–air batteries is limited by similar challenges, such as low power density, sensitivity to contaminants from air (e.g., $CO_2$), and electrolyte evaporation due to the open structure of air electrodes [84].

## RELATED RECENT REVIEWS

Several reviews related to metal–air batteries, including Li–air batteries, Zn–air batteries, electrolyte, air electrodes, and their electrocatalysts have been published [2], [3], [5]–[7], [13], [19], [52], [54], [82], [84]–[97]. In 1979, Blurton and Sammells published

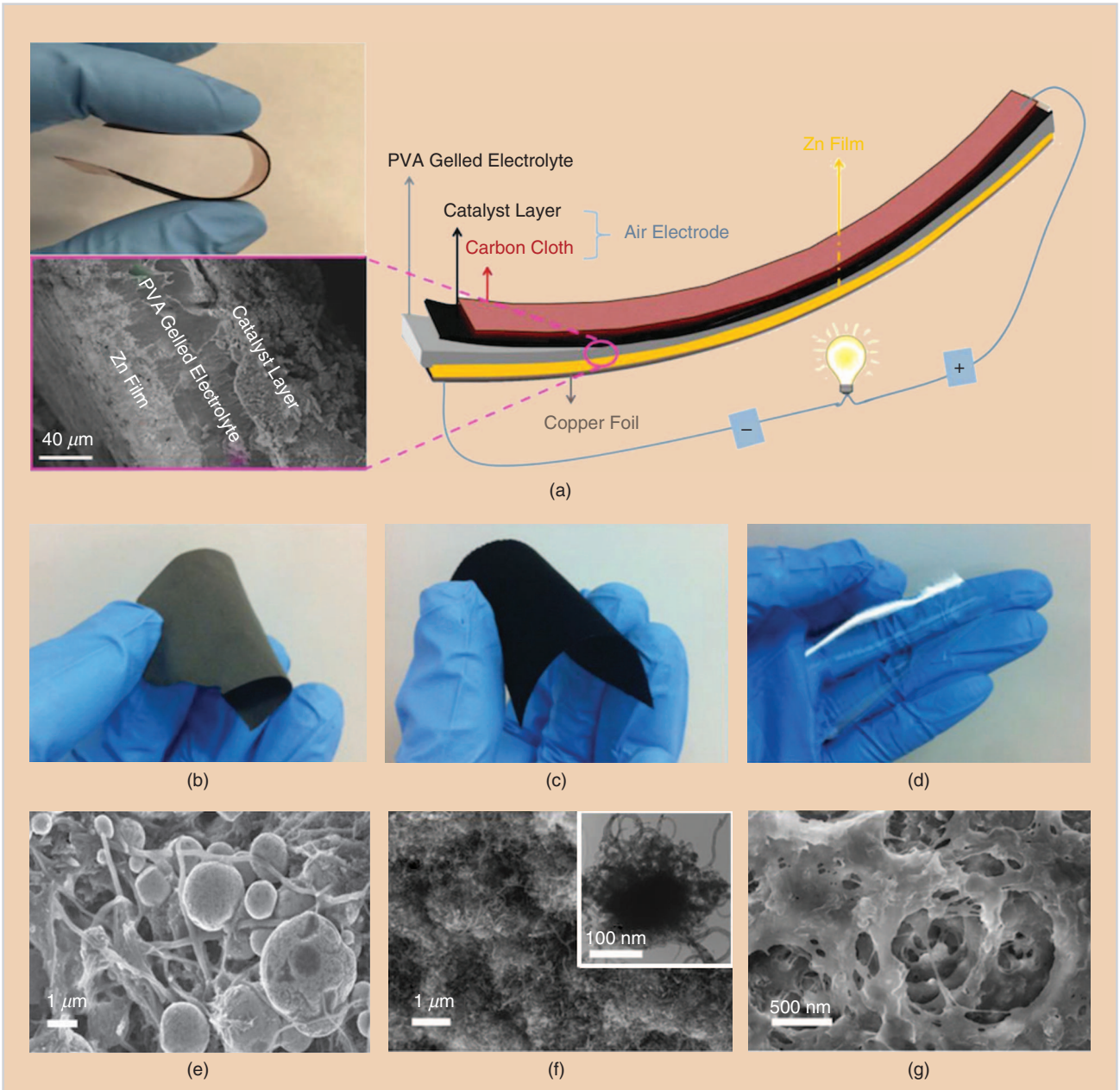


**FIGURE 5** (a) A schematic image of the solid-state, flexible, and rechargeable Zn–air battery. (The upper-left inset shows the flexibility of the cell, while the lower-left inset shows the cross-sectional scanning electron microscope (SEM) image of the laminated structure of the battery.] The optical pictures of (b) the freestanding Zn electrode film, (c) the bifunctional catalytic air electrode film using lanthanum Ni trioxygen ($LaNiO_3$)/nitrogen-doped (N-doped) carbon nanotubes (CNTs), and (d) the porous-gelled PVA electrolyte membrane. The corresponding SEM images of (e) the freestanding Zn film, (f) the bifunctional catalytic air electrode [the inset of the transmission electron microscope (TEM) image illustrates the core-corona structured $LaNiO_3$ nanoparticle and intertwined N-doped CNTs], and (g) the porous-gelled PVA electrolyte membrane. (Image and photos courtesy of Wiley-VCH Verlag GmbH and Co. KGaA, Weinheim.)

a review that concentrated on comparing Li, Al, Mg, Zn, and Fe/air batteries with a particular emphasis on the suitability of each system for electric vehicle propulsion [5]. In 2010, Girishkumar et al. at IBM published a perspective on Li–air batteries that summarized the promise and challenges facing development of practical Li–air batteries and the current understanding of their chemistry [13]. In 2011, Lee et al. provided a comprehensive list of Li–air and Zn–air batteries [3]. Cao et al. outlined some advancement in nonprecious ORR electrocatalysts for Li–air and Zn–air batteries in 2012 [84]. Christensen et al. published a review on the most critical challenges to develop robust, high-energy Li–air batteries and suggested future research directions to understand and overcome these challenges [90].

In 2012, Cheng and Chen published a review on oxygen electrochemistry

ORR involves complex steps, and the mechanisms may vary with different electrolytes and catalytic materials.

and electrocatalysts [6]. Bruce et al. provided a critical review on Li–air ($O_2$) and Li-S batteries. The article outlined the hurdles of energy storage and operation in nonaqueous and aqueous Li–air batteries [2]. Black et al. published a review on the electrocatalysts for ORR and OER and electrode and electrolyte materials for nonaqueous and hybrid Li–air batteries [89]. Shao et al. discussed the fundamental understanding of oxygen electrocatalysis in nonaqueous electrolytes and the status and challenges of oxygen electrocatalysts and provided a perspective on the design and development of new electrocatalysts in Li–air batteries [92]. Capsoni et al. published an article on the development of battery compartments in Li–air batteries [97]. In 2013, Wang et al. described electrocatalysts in metal–air batteries with aqueous or nonaqueous electrolyte [7]. Li et al. published a review discussing the current status, challenges, and perspectives of solid-state Li–air batteries [54]. Another review also provided by Li et al. presented the challenges in electrolyte, catalysts, and anodes of nonaqueous Li–air batteries [98]. Rahman et al. provided a comprehensive overview of the advances and challenges of metal–air batteries, including air cathode, electrolyte, and anode [85]. Shao et al. reported on the status and materials challenges for nonaqueous rechargeable Li–air batteries [19].

In 2014, Li et al. published a perspective on the development of nanostructured carbon-based electrocatalysts for nonaqueous Li-$O_2$ batteries [96]. In 2015, Manthiram and Li published a review on hybrid and aqueous Li–air batteries [52]. Wen et al. discussed the structure design of air electrodes in Li–air batteries [99]. In 2016, Mainar et al. provided a complete overview of Zn–air batteries, which focused on the alkaline aqueous electrolytes [82].

## ELECTROCHEMICAL REACTIONS OF AIR ELECTRODES

### *ORR*

The air electrode allows the oxygen from outside air to access the metal electrode continuously. It is usually composed of porous and electronically conductive support and high-surface-area catalysts for both ORR and OER and for the functional binder. The battery performance, including charge–discharge rate, capacity retention, energy efficiency, and cycling life [84], is strongly associated with the air electrode [93], [100] due to the electrocatalytic oxygen reaction (ORR/OER), which occurs at a three-phase contact zone between air, liquid electrolyte, and solid catalyst [101]. In particular, it involves ORR during discharge and OER during charge.

ORR involves complex steps, and the mechanisms may vary with different electrolytes and catalytic materials. In aqueous electrolyte, the ORR is associated with multistep electron transfer and complicated oxygen-containing species, such as O, OH, $O_2^-$, and $HO_2^-$ [102]–[104]. Furthermore, with alkaline electrolyte and metal catalysts, the related cathode reactions are thought to be described as follows [6]:

$$O_2 + 2H_2O + 4e^- \rightarrow 4OH^-, \quad [4e \text{ pathway}], \tag{4}$$

$$O_2 + H_2O + 2e^- \rightarrow HO_2^- + OH^-, \quad [2e \text{ pathway}], \tag{5}$$

$$HO_2^- + H_2O + 2e^- \rightarrow 3OH^-, \tag{6}$$

or

$$2HO_2^- \rightarrow 2OH^- + O_2. \tag{7}$$

The ORR under these conditions may proceed via a four-electron (4e) pathway (4) or a two-electron (2e) pathway (5). The direct 4e oxygen reduction is desirable due to its higher energy efficiency, while the 2e pathway produces peroxide species that can corrode and cause premature degradation of the battery [104]. The 2e pathway may be followed by either another further 2e reduction of peroxide (6) or a chemical disproportionation of peroxide (7). These processes can be described as a serial 2 × 2e pathway [102], [103]. In fact, the 4e and 2e pathways may occur concomitantly and compete with each other [6].

The ORR in nonaqueous electrolyte for Li–air batteries is receiving considerable attention. Laoire and coworkers found that ORR proceeds through a one-electron reversible process with $O_2/O_2^-$ redox coupled with large cations of tetrabutylammonium and tetraethylammonium [28].

### *OER*

OER is also the core reaction in Li–air and Zn–air batteries. Almost all OERs operate in alkaline conditions. The OER pathways are extremely complex. The elementary steps are believed to involve adsorbed OH and O species on the surface (*) according to the following scheme [105]:

$$OH^- + * \rightarrow OH^* + e^-, \tag{8}$$

$$OH^* + OH^- \rightarrow O^* + H_2O + e^-, \tag{9}$$

$$O^* + O^* \rightarrow O_2, \tag{10}$$

$$O^* + OH^- \rightarrow OOH^* + e^-, \tag{11}$$

$$OOH^* + OH^- \rightarrow O_2 + H_2O + e^-. \tag{12}$$

The evolution of $O_2$ is thought to involve one of the two pathways, including the direct reaction (10) and two-step reactions of (11) and (12). Furthermore, the latter pathway is thought to occur more easily because the thermodynamic barrier for reaction (10) is always larger by theoretical investigations [106], [107].

Bajdich and colleagues studied the OER of cobased oxide surfaces experimentally,

and the theoretical investigations show that $\beta$-CoOOH is the active phase where the OER occurs in alkaline media. They further calculated the relative surface stabilities and adsorbate coverages of the most stable low-index surfaces of $\beta$-CoOOH: (0001), $(01\bar{1}2)$, and $(10\bar{1}4)$. At low applied potentials, the $(10\bar{1}4)$ surface is the most stable, while the $(01\bar{1}2)$ surface is the more stable at higher potentials [105]. Trasatti reported that the enthalpy of transition from the next lower oxide to the nominal oxide could be used as the OER activity descriptor [108]. Bockris and Otagawa measured the OER on 18 substituted perovskites containing first-row transition-metal ions. They found the electrode kinetics increase with the decrease of the enthalpy of formation of the transition-metal hydroxides and with the increase in the number of d electrons in the transition-metal ions [109].

Rossmeisl et al. investigated the trends in the electrocatalytic properties of surfaces of three rutile-type oxides, including ruthenium oxide ($RuO_2$), iridium oxide ($IrO_2$), and titanium dioxide ($TiO_2$), using discrete Fourier tranform calculations [110]. They established that rutile oxide surfaces obey linear relations between $O^*$ binding energy and the binding energy of two other species relevant to $HO^*$ and $HOO^*$. Furthermore, it is possible to describe trends in the OER activity through a volcano curve showing the activity as a function of the binding energy of O to the surface [110], [111]. Although some OER activity descriptors were proposed, identifying the efficient electrocatalysts for OER remains a key challenge in metal–air batteries.

## OXYGEN ELECTROCATALYSTS FOR LI–AIR AND ZN–AIR BATTERIES

### *TRANSITION-METAL OXIDES*

Transition-metal oxides are considered as an alternative to traditional noble-metal electrocatalysts for metal–air battery applications because of reasonable activity and stability in alkaline electrolyte, low cost, widespread availability, and environmental friendliness [88], [112].

Among them, $MnO_x$ with good ORR activity has attracted the most research interest in nonaqueous Li–air batteries [113]–[115]. Since the first report of an $MnO_2$ catalyst for ORR in the early 1970s [116], many efforts have been made to promote the development of highly active $MnO_x$-based catalysts involving the structure, morphology, composition, valence, and electrical conductivity [117]–[119]. The catalytic performance of $MnO_2$ strongly associates with the crystallographic structure, following a decreasing order of $\alpha$->$\beta$->$\gamma$-$MnO_2$ [120]. Moreover, the morphology of $MnO_2$ also affects the catalytic activity. Débart et al. found that the use of $\alpha$-$MnO_2$ catalyst with nanowire morphology in an oxygen cathode for rechargeable Li-$O_2$ batteries could deliver the higher capacity of 3,000 mAh/g of carbon over that of the bulk $\alpha$-$MnO_2$ (see Figure 6 [121]). Mao et al. and Brenet investigated the composition's effect on the performance in the ORR, following the sequence of $Mn_5O_8$ < $Mn_3O_4$ < $Mn_2O_3$ < MnOOH [117], [122], [123].

Another key factor in controlling the catalytic performance of ORR is valence. The $MnO_x$ catalysts with higher Mn valence often exhibit better catalytic activity [124]. Suntivich et al. demonstrated that the ORR activity of oxide catalysts primarily correlates to $s^*$-orbital occupation and the extent of B-site transition-metal-oxygen covalency, which serves as a secondary activity descriptor (Figure 7). They further found that increase of hybridization positively affects ORR activity, as shown in Figure 8 [125]. To further improve the performance, some multivalence transition metals, e.g., cobalt (Co), were doped into the $MnO_x$-based catalysts [93], [126]–[129]. Furthermore, more transition metals, such as Al, Fe, chromium (Cr), and lanthanum (La), were doped into $MnO_x$ and lead to the formation of mixed-metal oxides on a spinel, perovskite, and pyrochlore structure. Spinels are a group of oxides with the general formula $A^{2+}B^{3+}{}_2O^{2-}{}_4$ (A = Mg, Fe, Co, Ni, Mn, or Zn; B = Al, Fe, Co, Cr, Mn; and so on) [7], [130]. Spinel-typed oxides usually could provide mixed valence in the cations, act as the

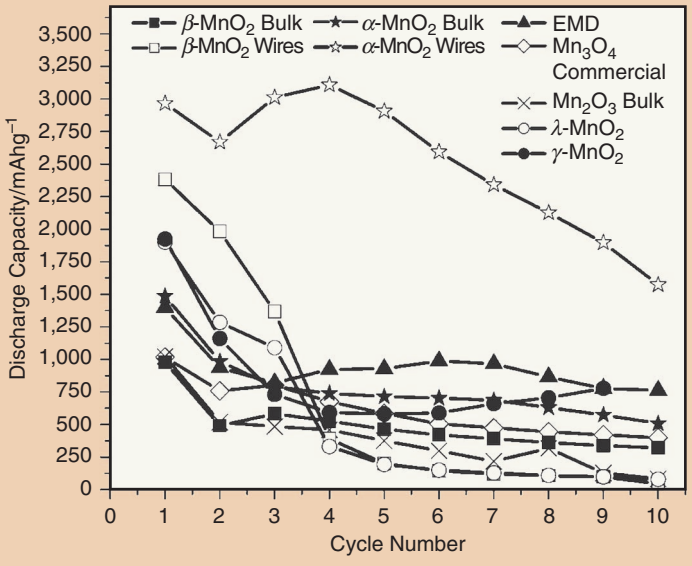


**FIGURE 6** A variation of discharge capacity with cycle numbers for several porous electrodes containing $MnO_2$ as catalysts: $\alpha$-$MnO_2$ in bulk and nanowire form, $\beta$-$MnO_2$ in bulk and nanowire form, $\gamma$-$MnO_2$, $\lambda$-$MnO_2$, $Mn_2O_3$, and $Mn_3O_4$. Electrolytic MnO2 (EMD) is included herein for comparison but was reported previously in [12]. Cycling was carried out at a rate of 70 mA/g in one atmosphere of $O_2$. Capacities are per gram of carbon in the electrode. Lower cutoff potential 2 V. (Image from [12], used with permission.)

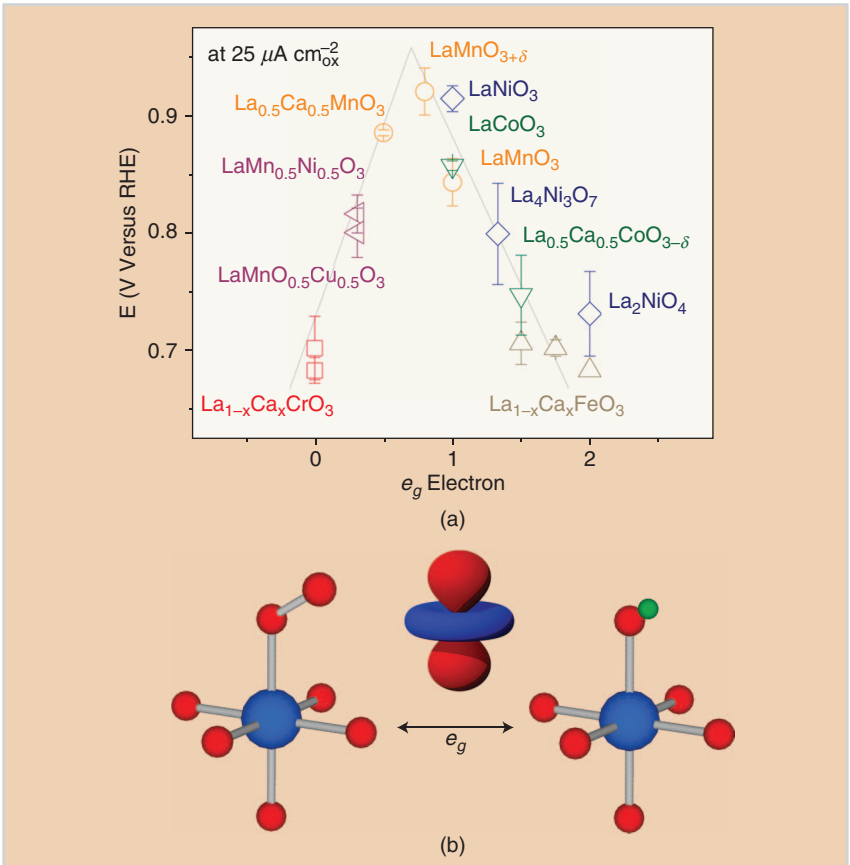


**FIGURE 7** The role of $e_g$ electron on ORR activity of perovskite oxides. (a) The potentials at 25 mA cm$^{-2}_{ox}$ as a function of e orbital in perovskite-based oxides. Data symbols vary with type of boron (B) ions [chromium (Cr), red; Mn, orange; Fe, grey; cobalt (Co), green; Ni, blue; mixed compounds, purple], where x = 0 and 0.5 for Cr and 0, 0.25, and 0.5 for Fe. Error bars represent standard deviations (SDs). (b) The shape of the electron points directly toward the surface O atom and plays an important role during $O_2^{2-}/OH^-$ exchange. O, B, and H atoms are colored red, blue, and green, respectively. RHE: reversible hydrogen electrode. (Figure courtesy of Macmillan Publishers Limited.)

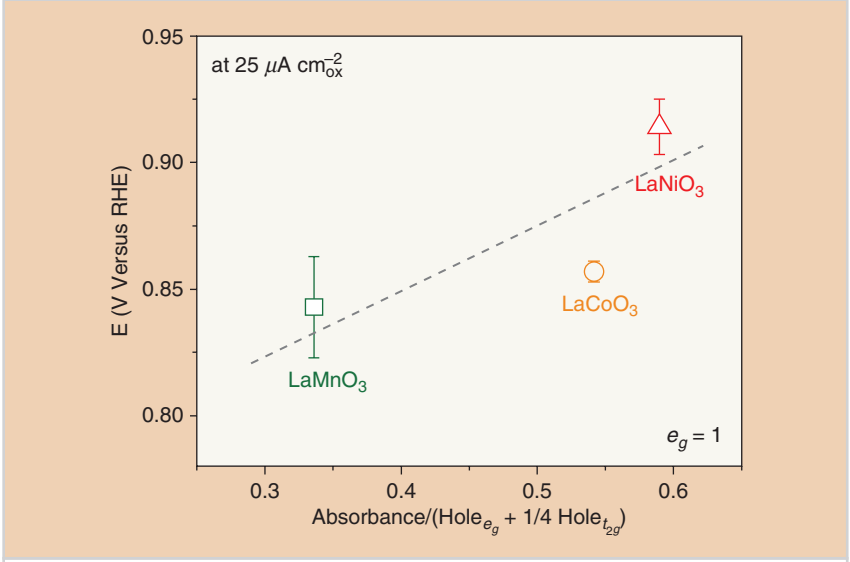


**FIGURE 8** The role of B-O covalency on the ORR activity of perovskite oxides. The potentials at 25 mA cm$^{-2}_{ox}$ as a function of the B-O covalency, which is estimated by the oxnormalized absorbance at $e_g$-filling = 1. (Figure courtesy of Macmillan Publishers Limited.)

acceptor/donor chemisorption sites for oxygen, and assist the electron transfer to exhibit electric conductivity or semiconductivity [131], [132]. It promotes the performance of ORR and OER in alkaline medium [133]–[139].

Zhao et al. obtained spinel Mn–Co oxide nanoparticles partially embedded in the nanotubes by concurrently rupturing nitrogen-doped (N-doped) carbon nanotubes (CNTs) and oxidizing Co and Mn nanoparticles. The catalyst shows high dual activity for oxygen reduction and evolution, surpassing that of carbon-supported platinum (Pt) (Pt/C), $RuO_2$, and $IrO_2$ [140]. Li et al. reported a general synthesis of ultrasmall CoMn spinels with tailored structural symmetry and composition through a facile solution-based oxidation-precipitation and insertion-crystallization process in modest conditions. The as-synthesized c-$CoMn_2/C$ composite shows superb electrocatalytic activity and stability for ORR and OER. The assembled primary Zn–air batteries exhibit stable galvanostatic discharge curves, giving a high energy density of ~650 Wh kg$^{-1}$ at 10 mA cm$^{-2}$ normalized to consumed Zn anode. The average voltage of discharge platform decreases by 8.5% after 155 cycles, half that of Pt/C (Figure 9) [141].

Innovative technologies to prepare high-performance catalysts are of great importance. Cheng et al. have developed a rapid methodology at room temperature based on reduction-recrystallization of amorphous $MnO_2$ precursors in an aqueous solution containing $Co^{2+}$ ions to selectively synthesize the spinel nanocrystalline $Co_3Mn_{3-x}O_4$ as a high active bifunctional catalyst in ORR and OER. The ORR performances of the four spinel samples were comparable with the benchmark Pt/C catalyst. Furthermore, the most active CoMnO-P was used to construct a Zn–air battery, which delivered a stable galvanostatic discharge curve and considerable specific energy densities [142].

Another structure of bifunctional catalysts in alkaline electrolytes is perovskite-type oxides that have the general formula $ABO_3$, where A is the larger cation, such as a rare earth or an

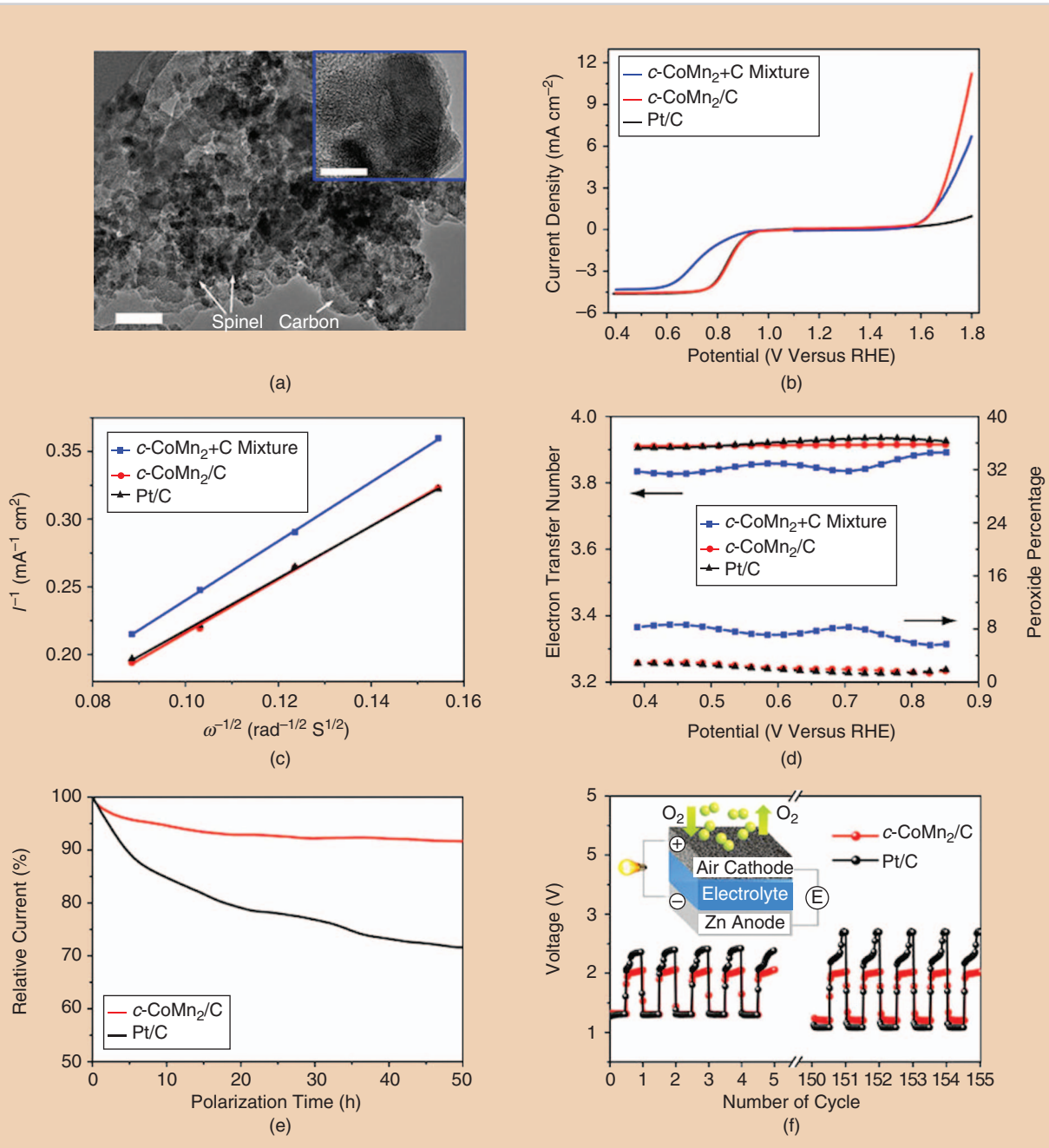


**FIGURE 9** A carbon-supported CoMnO spinel for ORR/OER and metal–air batteries. (a) A TEM image of prepared *c*-$CoMn_2$/C hybrid. The scale bar is 50 nm. The inset shows firm anchoring of a single spinel nanoparticle on carbon. The scale bar is 10 nm. (b) A comparison of ORR and OER activities of a *c*-$CoMn_2$+C mixture, *c*-$CoMn_2$/C hybrid, and Pt/C catalyst in a 0.1 M potassium hydroxide (KOH) solution. The rotation rate is 900 r/min during the ORR. (c) K-L plots at 0.65 V. (d) The electron transfer number and peroxide percentage generated at various potentials. (e) Chrono-amperometric responses of *c*-$CoMn_2$/C and Pt/C at 0.8 V in $O_2$-saturated 0.1-M KOH. (f) The performance of rechargeable Zn–air cells based on *c*-$CoMn_2$/C and Pt/C catalysts at a cycling rate of 10 mA $cm^{-2}$ and a duration of 400 s per cycle. The inset schematically depicts the structure of assembled rechargeable Zn–air cells. (Images and photo courtesy of Macmillan Publishers Limited.)

alkaline earth element, and B is generally a transition metal with smaller size [143]. The catalytic activity can be tuned by partially or fully substituting A and B cations with other metals [144], [145]. The substituted perovskites have an $A_{1-x}A'_xB_yB'_{1-y}O_3$ formula. In general, the substitution of A site and B site mainly affects the stability and activity of adsorbed oxygen, respectively [7], [146]. In $LaNi_{0.92}Mg_{0.08}O_3$ and $LaNi_{0.85}Mg_{0.15}O_3$ catalysts, Du et al. reported that the partial substitution of Ni with Mg improved the ORR performance compared to $LaNiO_3$ catalyst in nonaqueous Li–air batteries [145].

Besides the ORR, transition-metal oxides are of particular interest due to

Transition-metal oxides are of particular interest due to their intrinsic activities comparable to the gold standards of OER catalysts.

their intrinsic activities comparable to the gold standards of OER catalysts, such as $IrO_2$ and $RuO_2$, which are highly active but precious. Among the catalytically nonprecious metal oxides, $MnO_x$ films as OER catalysts have been extensively studied in neutral and alkaline solutions [147]–[151]. Robinson et al. systematically compared the eight synthetic oxide structures containing Mn(III) and Mn(IV) and found the catalytic activities decrease in the series $Mn_2O_3 > Mn_3O_4 \gg \lambda$-$MnO_2$ [150]. However, the first-row transition-metal oxides, especially of Ni, Co, and Mn, are typically considered to be of lower activity [152]–[166]. The inherent and not very good conductivities of most of the transition-metal oxides limit their activities for the OER, because the M–O bond strength is either too strong or too weak, thereby slowing the rate-limiting step [111]. To improve the activity, transition-metal oxyhydroxides of the same elements were investigated.

Zou et al. and Subbaraman et al. have used well-characterized $M^{2+\delta}O^{\delta}(OH)_{2-\delta}/Pt(111)$ catalyst surfaces (M = Ni, Co, Fe, Mn) to establish clear trends in activity for the OER of a complex oxide system. They reported the $OH_{ad}$-$M^{2+\delta}$ interaction could be used as the primary descriptor of the activity for OER for these 3-$\delta$-M hydr(oxy) oxide systems, which follow the order Ni > Co > Fe > Mn (Figure 10) [147], [167]. Bediako et al. studied the Ni-borate film catalysts for OER by in situ X-ray absorption spectroscopy and found evidence for the formation of such metal hydroxides. Furthermore, they reported the clear

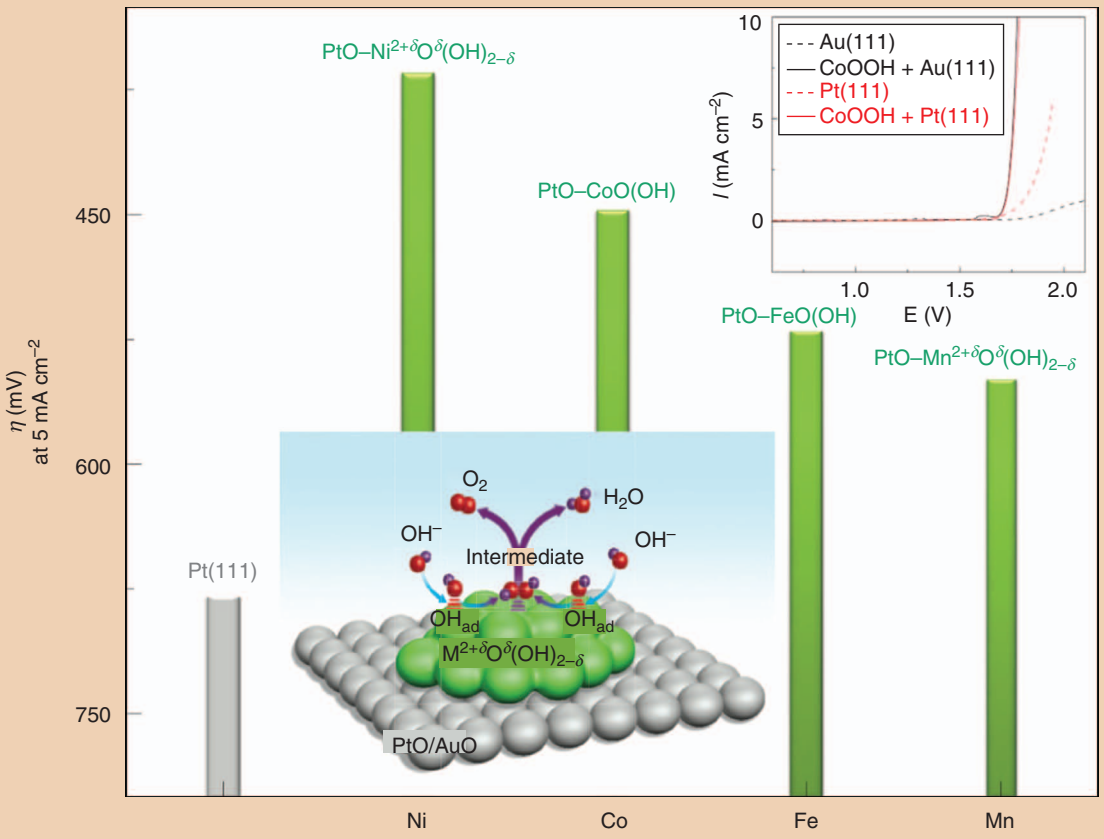


**FIGURE 10** The trend in overpotential for the OER is shown as a function of the 3-$\delta$ transition elements. The elements are arranged in the order of their oxophilicity from Mn to Ni. Pt is shown in the figure as a reference. The top inset shows a comparison of polarization curves for Pt(111) and Au(111) with 40% CoOOH for the OER. Au: gold. The two potential curves are identical, suggesting a limited or no role played by the noble-metal substrate for this reaction. As a result, this reaction is classified as a monofunctional reaction, and the main descriptor (as can be clearly seen from the trend) is still the $OH_{ad}$-$M^{3+}$ interaction. The bottom inset shows a schematic of the OER. $OH^-$ from the bulk is found to adsorb on the free catalyst site on the oxide clusters. The adsorbed OH groups $OH_{ad}$ react with other such groups to form a reaction intermediate (recombination), which is then further oxidized to $O_2$ and $H_2O$. (Image courtesy of Macmillan Publishers Limited.)

**TABLE 1** A summary of the OER activities of the various catalysts electrocatalytic parameters of Li transition metal oxides before and after electrochemical tuning and 20 wt Ir/C catalysts.

| SAMPLE | POTENTIAL AT 0.1 MA CM$^{-2}$ (V VERSUS RHE) | POTENTIAL AT 5 MA CM$^{-2}$ (V VERSUS RHE) | TAFEL SLOPES (MV DEC$^{-1}$) | SAMPLE | POTENTIAL AT 0.1 MA CM$^{-2}$ (V VERSUS RHE) | TAFEL SLOPES (MV DEC$^{-1}$) |
|---|---|---|---|---|---|---|
| De-$LiCoO_2$ | 1.525 ± 0.01 | 1.61 ± 0.01 | 50 ± 3 | $LiCoO_2$ | 1.59 ± 0.01 | 48 ± 5 |
| De-$LiCo_{0.5}Ni_{0.5}O_2$ | 1.52 ± 0.01 | 1.6 ± 0.01 | 42 ± 4 | $LiCo_{0.5}Ni_{0.5}O_2$ | 1.56 ± 0.01 | 50 ± 3 |
| De-$LiCo_{0.5}Fe_{0.5}O_2$ | 1.5 ± 0.01 | 1.565 ± 0.01 | 40 ± 4 | $LiCo_{0.5}Fe_{0.5}O_2$ | 1.56 ± 0.01 | 47 ± 5 |
| De-$LiCo_{0.33}Ni_{0.33}Fe_{0.33}O_2$ | 1.47 ± 0.01 | 1.525 ± 0.01 | 35 ± 3 | $LiCo_{0.33}Ni_{0.33}Fe_{0.33}O_2$ | 1.55 ± 0.01 | 45 ± 4 |
| De-$LiCo_{0.33}Ni_{0.33}Mn_{0.33}O_2$ | 1.54 ± 0.01 | 1.625 ± 0.015 | 48 ± 4 | $LiCo_{0.33}Ni_{0.33}Mn_{0.33}O_2$ | 1.57 ± 0.01 | 45 ± 5 |
| 20 wt Ir/C | 1.46 ± 0.01 | 1.545 ± 0.01 | 46 ± 4 | | | |

De: delithiated. (Table courtesy of Macmillan Publishers Limited.)

correlations of the $\beta$-NiOOH structure to OER activity [168].

Other reports indicate that mixed transition-metal oxides are also the material choice as nonprecious OER catalysts [88], [109], [156], [169]. Boettcher et al. investigated the OER activities of thin films of $NiO_x$, $CoO_x$, $Ni_yCo_{1-y}O_x$, $Ni_{0.9}Fe_{0.1}O_x$, $IrO_x$, $MnO_x$, and $FeO_x$. And the $Ni_{0.9}Fe_{0.1}O_x$ was found to be the highest activity with 10 mA cm$^{-2}$ at an overpotential of 336 mV in basic media [170]. Lu et al. demonstrated a method for electrochemical Li tuning of catalytic materials by continuously extracting Li-ions out of $LiCoO_2$ and other cobased compounds. They studied several mixed metal oxides and found the activity of delithiated $LiCo_{0.33}Ni_{0.33}Fe_{0.33}O_2$ shows the best OER performance with onset potentials of ~1.47 V at 10 mA cm$^{-2}$, as shown in Table 1 [253]. The nanocrystalline spinels, mainly composed of manganese [171], [172] or Co [173] and perovskites [174], [175], are usually considered as the more active OER electrocatalysts.

A fundamental understanding of the links between materials properties and catalytic activity can assist the design and development of highly active oxide catalysts [125], [176]. Suntivich et al. demonstrated that the OER activity exhibits a volcano-shaped dependence on the occupancy of the 3-$\delta$ electron with an $e_g$ symmetry of surface transition-metal cations in an oxide. Furthermore, the peak OER activity was predicted to be at an $e_g$ occupancy close to unity, with high covalency of transition-metal–oxygen bonds. This design principle helps the prediction of highly active $Ba_{0.5}Sr_{0.5}Co_{0.8}Fe_{0.2}O_{3-d}$ catalyst, and the experimental OER activity is at least one order of magnitude higher than that of the state-of-the-art iridium oxide catalyst in alkaline media (see Figure 11) [174].

Development of bifunctional electrocatalysts remains a great challenge [6], [91], [177]. Yoon et al. exploited two types of double-walled $RuO_2$ and $Mn_2O_3$ composite fibers as the bifunctional catalyst. They show enhanced overpotential characteristics and stable cyclability over 100 cycles in the Li–$O_2$ battery [178]. Pyrochlore is a family of oxides that reduces the active overpotentials both in ORR and OER [179] with the general formula $A_2B_2O_6O'_{1-\delta}$ (A = Pb, Bi; B = Ru, Ir) [180]. Its unusual framework links to

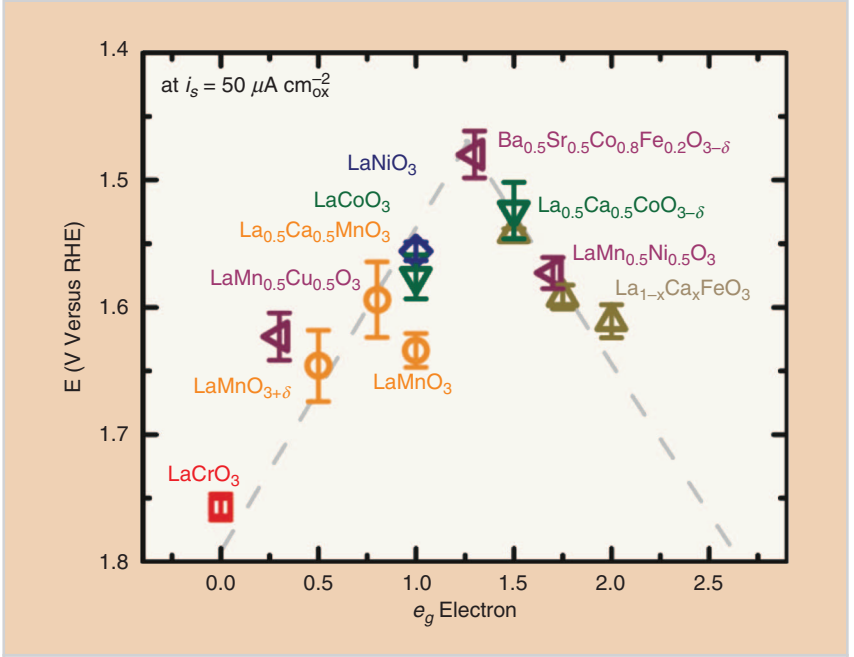


**FIGURE 11** The relation between the OER catalytic activity, defined by the overpotentials at 50 mA cm$^{-2}$ of OER current, and the occupancy of the $e_g$-symmetry electron of the transition metal (B in $ABO_3$). Data symbols vary with type of B ions (Cr, red; Mn, orange; Fe, beige; Co, green; Ni, blue; mixed compounds, purple), where x = 0, 0.25, and 0.5 for Fe. Error bars represent SDs of at least three independent measurements. The dashed volcano lines are shown for guidance only. (Figure courtesy of American Association for the Advancement of Science.)

the properties. For $Pb_2Ru_2O_6O'_{1-\delta}$, e.g., metal oxygen octahedra ($RuO_6$) form cages that provide facile electronic conduction paths and result in metallic conductivity up to $1 \times 10^3$ S cm$^{-2}$. Special oxygen atoms (O′) are located in Pb-O′-Pb bridges. The complete or partial absence gives rise to oxygen nonstoichiometry, which is accommodated by variable metal valence [181]–[184]. According to these factors, Oh et al. developed a novel metallic pyrochlore oxide with a composition of $Pb_2[Ru_{1.6}Pb_{0.44}]O_{6.5}$ as the bifunctional catalyst. It has high performance of reversible capacities up to 10,300 mAh g$^{-1}$ in Li–air batteries (Figure 12) [181].

The electrocatalytic potential of most transition-metal oxides is impaired by their poor electronic conductivity. However, it may be improved by doping the oxides with electron donors or by supporting the nonconducting materials.

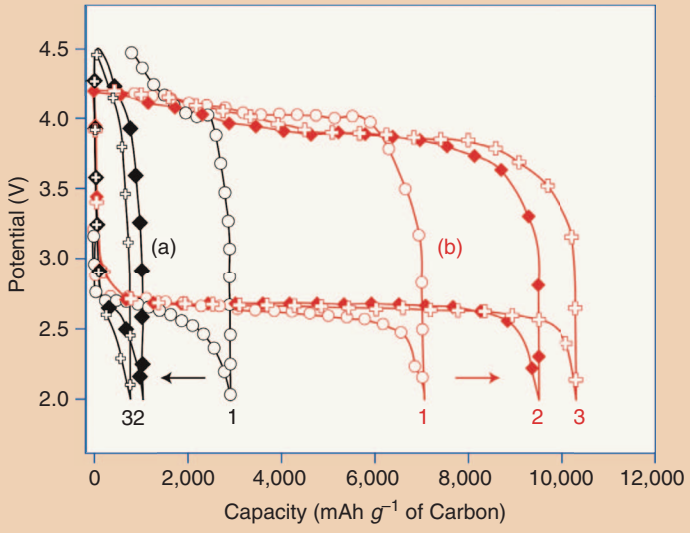


**FIGURE 12** The discharge–charge profiles of the first three cycles for carbon in $LiPF_6$/tetraethylene glycol dimethyl ether [(a), black] and MP pyrochlore [(b), red], with cycle sweeps as indicated (the current rate is 70 mA g$^{-2}$ of carbon). (Figure courtesy of Macmillan Publishers Limited.)

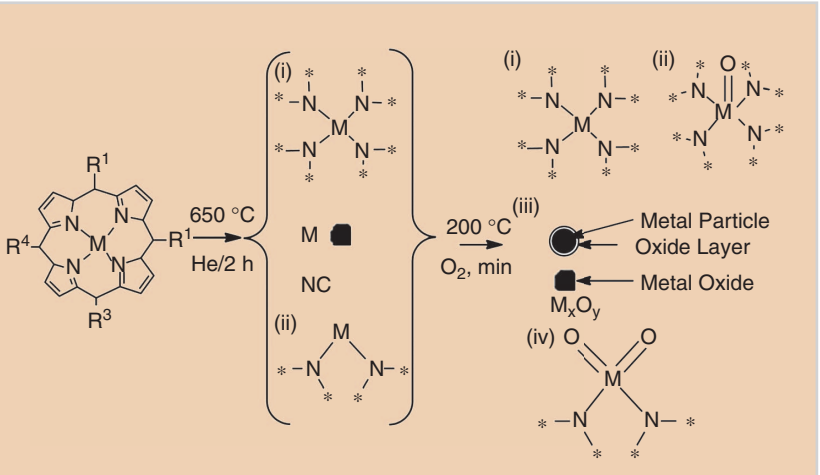


**FIGURE 13** A schematic illustration of the possible groups that are formed during pyrolysis of Co and Mn $N_4$-metallomacrocyclic complexes at 650 °C for 2 h under helium (He) and subsequent calcination in oxygen at 200 °C for 30 min. (Figure courtesy of Wiley-VCH Verlag GmbH and Co. KGaA, Weinheim.)

## INORGANIC–ORGANIC HYBRID MATERIALS

To improve the conductivity of transition-metal oxides, one of the strategies is the development of metal-oxide–carbon hybrid materials in which the oxide catalysts are firmly combined with highly conducting substrates for oxygen electrochemistry [112], [185]–[187]. These materials include transition-metal macrocycles, transition-metal polymer composites, transition-metal nitrides, and metal-oxide–nanocarbon hybrid materials.

Since 1964, $N_4$-chelate complex with a Co metal center was reported as the ORR catalyst, and much research on transition-metal macrocycles with the feature of transition-metal centers (Co, Fe, Ni, or Mn) coordinated to some surrounding nitrogen atoms (simply labeled as M-$N_x$/C, x is normally 2 or 4) has been done [112], [188]. The active sites of these materials for ORR are believed to correlate with the transition-metal centers that transfer the electron to $O_2$ $O_2p^*$ orbital, weaken the O–O band, and further improve the ORR performance [187]–[193]. Furthermore, the stability as well as activity of transition-metal macrocycles for ORR catalysis could be significantly improved by heat treatment [194], [195]. Jahnke and coworkers found that all of the heat-treated carbon-supported CoTAA (dihydrodibenzotetraazaannulene) catalyst showed better stability and activity than untreated samples [196].

Masa et al. embedded $Mn_3O_4$ $Co_3O_4$ nanoparticles into the nitrogen-doped carbon by selective prolysis and mild calcination of manganese and Co $N_4$ complex. And the $Mn_xO_y$/NC and $Co_xO_y$/NC showed much lower overvoltages of the OER and ORR compared to those of the state-of-the art catalysts $RuO_2$, $IrO_2$, and Pt/C. As shown in Figure 13, a number of species were proposed that result from the heat treatment of Co and manganese $N_4$-metallomacrocyclic complexes, such as M-$N_x$ moieties, metal, metal

oxides, and nitrogen-functionalized carbon groups. The exceptional efficiency of ORR and OER was attributed to the nitrogen-functionalized carbon groups and the spinels of the respective metals [197]. Plasma thermal treatment method as a new heat treatment technology was developed to suppress particle aggregation and increase surface area of macrocycle catalysts during the synthesis process. Furthermore, it also could improve the activity [198].

Besides the heat treatment, enormous efforts have been devoted to the design and synthesis of new structural macrocycles, including sigle macrocycle [199] and cofacial macrocyclic dimers [200]–[202], among others. Liu et al. developed a carbon-supported $[CoN_4]_3$ catalyst in which triangular trinuclear metal-$N_4$ complexes were combined with a planar conjugated macrocycle, and it showed much better electrochemical activity and long-term stability than the commercially available Pt/C catalyst in alkaline electrolytes [203]. Several multimetallic nitrides supported on N-doped carbon materials were designed and synthesized to improve the ORR performance [204]–[207].

In ORR performance, there is often a tradeoff between the catalytic activity and stability. Easton and coworkers have investigated the composition effect for the activity and stability of $M_xC_{1-x-y}N_y$ catalysts (M = V, Cr, Mn, Fe, Co, and Ni). They found that the activity could be tuned by the transition metals. For example, in acid solutions, the activity follows the order Fe > Co > Cr > Ni, and N element increases the activity [208], [209]. Among them, the $Cr_xC_{1-x-y}N_y$ catalysts show good stability of corrosion resistance [210]. The results indicate that the tradeoff relationship could be optimized by the adjustment of the metal centers.

Conductive polymers [polyaniline (PANI), PY, PT, and derivates] and oxidized metallic particles deposited on carbons tend to enhance the performance [211]. Pyrolized metal porphyrins with the precursors of Co and Fe porphyrins have attracted the most attention over the years. The Co-polypyrrole composite catalyst (Co-PPy-C) synthesized via a pyrolysis-free process delivers high ORR activity without any notable loss [212]. Prabu et al. reported that the metal nitrate/polyacrylonitrile (PAN) and metal acetylacetonate/PAN could be used as the precursor, and one-dimensional (1-D) $NiCo_2O_4$ (NCO) nanostructures (Figure 14) were prepared by using a simple electrospinning technique. The NCO catalyst shows extraordinary bifunctional catalytic activity toward both ORR and OER in Zn–air batteries with the low overpotential of 0.84 V. The ORR onset potential is 0.93 V [versus standard hydrogen electrode (SHE)], and the OER performance displays a current density of –10 mA $cm^{-2}$ at 1.62 V [213]. The heteroatom polymer, PANI, as both the nitrogen and carbon source process was graphitized with the catalysis of a Co species. Moreover, the PANI facilitates the graphitization and forms N-doped graphene-sheetlike structures. The prepared graphene-rich catalysts (Co-N-MWNTs) exhibit superior ORR activity in nonaqueous Li-$O_2$ battery systems [214].

Transition-metal nitrides are well-known catalysts in ORR in aqueous electrolytes [93]. To further improve their activity, conductive carbon substrates, such as activated carbon, CNTs, or graphene, are incorporated to the metal nitrides [96] or metal oxides. Chen et al. designed CCBC that consists of lanthanum nickelate centers supporting N-doped CNTs for rechargeable Zn–air batteries (see Figure 15). After full-range degradation tests, CCBC retained excellent activity of three and 13 times greater current densities of ORR and OER upon comparison to state-of-the-art Pt/C, respectively [215].

Another type of bifunctional electrocatalyst was developed based on two- to three-walled CNT-graphene complexes. The outer walls of the CNTs were partially unzipped to create nanoscale sheets of graphene attached to the inner tubes. And the nitrogen impurities and extremely small amounts of Fe in the sheets were beneficial for the catalytic sites and boosted the activity. The inner walls remained intact and retained their electrical conductivity, which facilitated charge transport during electrocatalysis. In acidic solutions, the catalyst exhibits high ORR activity and superior stability, and in alkaline solutions, its ORR activity closely approaches that of Pt (Figure 16) [216].

Wang et al. synthesized the $MnCo_2O_4$-graphene hybrid material by direct nucleation and growth of $MnCo_2O_4$ nanoparticles on reduced graphene oxide. The hybrid material with inherited excellent catalytic activity shows lower overpotentials and longer cycle lives than that of Pt catalyst in Li–air batteries [217].

Using the same synthesis method, the $MnCo_2O_4$ nanoparticles were grown on the N-doped reduced graphene oxide (N-rmGO). This revealed that the C-O-metal and C-N-metal bonds afforded much greater activity and durability than the physical mixture of nanoparticles and N-rmGO in alkaline solutions [127]. They further improve ORR performance of the little-active $Co_3O_4$ nanoparticles by growing the nanoparticles on N-rmGO. The hybrid exhibits

Metal-organic frameworks are a new type of functional material featuring high surface area, tunable pore sizes, structural diversity, and designable functionality.

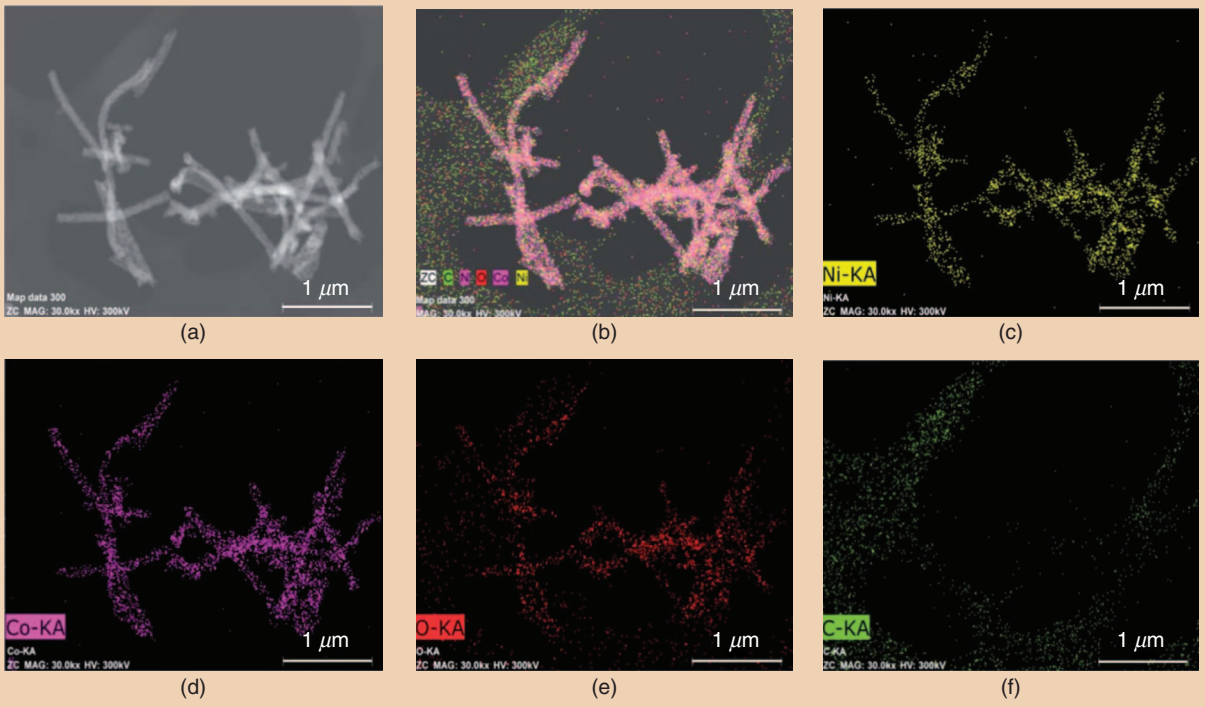


**FIGURE 14** (a) The bright field TEM image of NCO-$A_1$ shows the 1-D structure morphology; (b) the overlay image and the corresponding EDX maps depict the distribution of constituting individual elements within the nanostructure as shown in (c)–(f). The images correspond to the (c) Ni-K edge (Ni-KA), (d) Co-K edge (Co-KA), (e) oxygen-K edge (O-KA), nitrogen-K edge (N-KA), and (f) carbon-K edge (C-KA). (Photos courtesy of the Royal Society of Chemistry.)

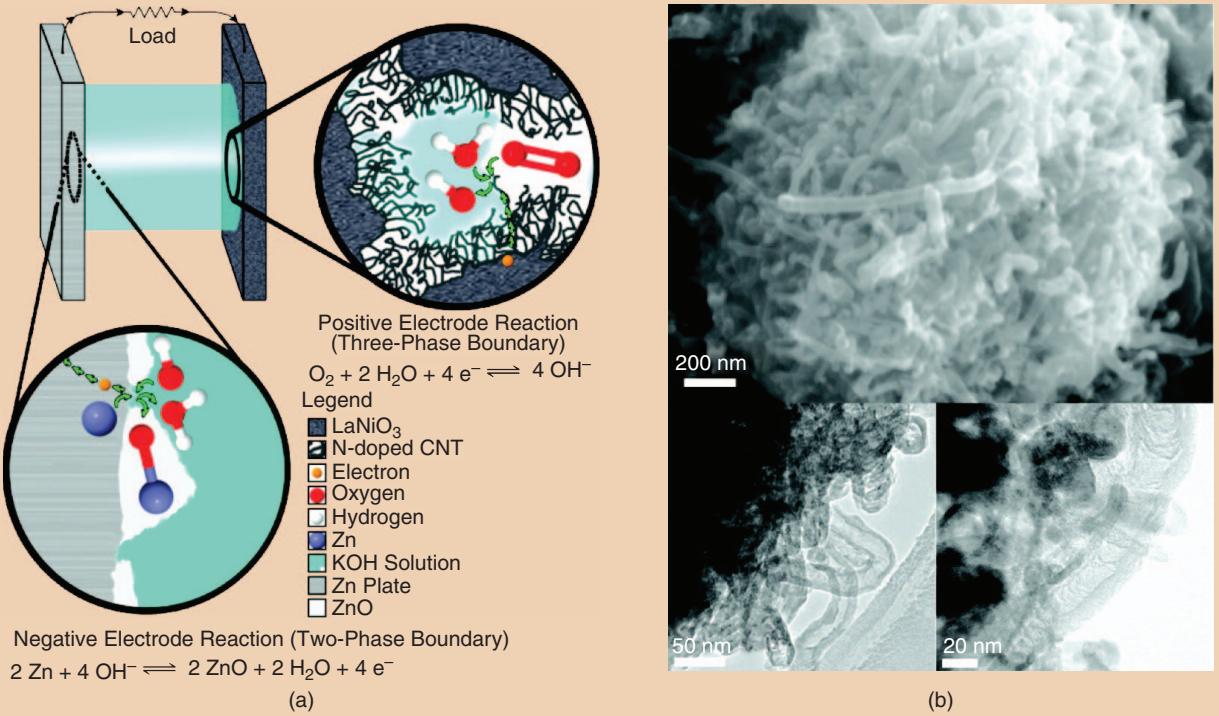


**FIGURE 15** The design and application of the core-corona structured bifunctional catalyst (CCBC) toward metal–air battery. (a) A schematic of Zn–air battery and the reactions taking places on the electrodes. The CCBC catalyst is applied to the positive electrode, which catalyzes the ORR and OER reactions. (b) The SEM and TEM of the CCBC illustrating the N-doped CNT on the surface of the core particle. (Image and photo courtesy of American Chemical Society.)

comparable ORR catalytic activity to a commercial Pt/C catalyst and superior stability and could act as a new bifunctional catalyst for ORR and OER [218]. Furthermore, the authors developed a CoO/CNT hybrid ORR catalyst and Ni-Fe-layered double hydroxide (LDH) OER catalyst in a Zn–air battery, as shown in Figure 17. These catalysts showed higher catalytic activity and durability in concentrated alkaline electrolytes than precious Pt and Ir catalysts. The Zn–air batteries exhibited an unprecedented small charge–discharge voltage polarization of ~0.70 V at 20 mA $cm^{-2}$, high reversibility, and stability over long charge and discharge cycles [58].

Metal-organic frameworks (MOFs) are a new type of functional material featuring high surface area, tunable pore sizes, structural diversity, and designable functionality [219]–[222]. MOFs or their derived nanostructures are one of the hottest research points in electrocatalysts [223], [224]. Zhang et al. reported the doped carbon

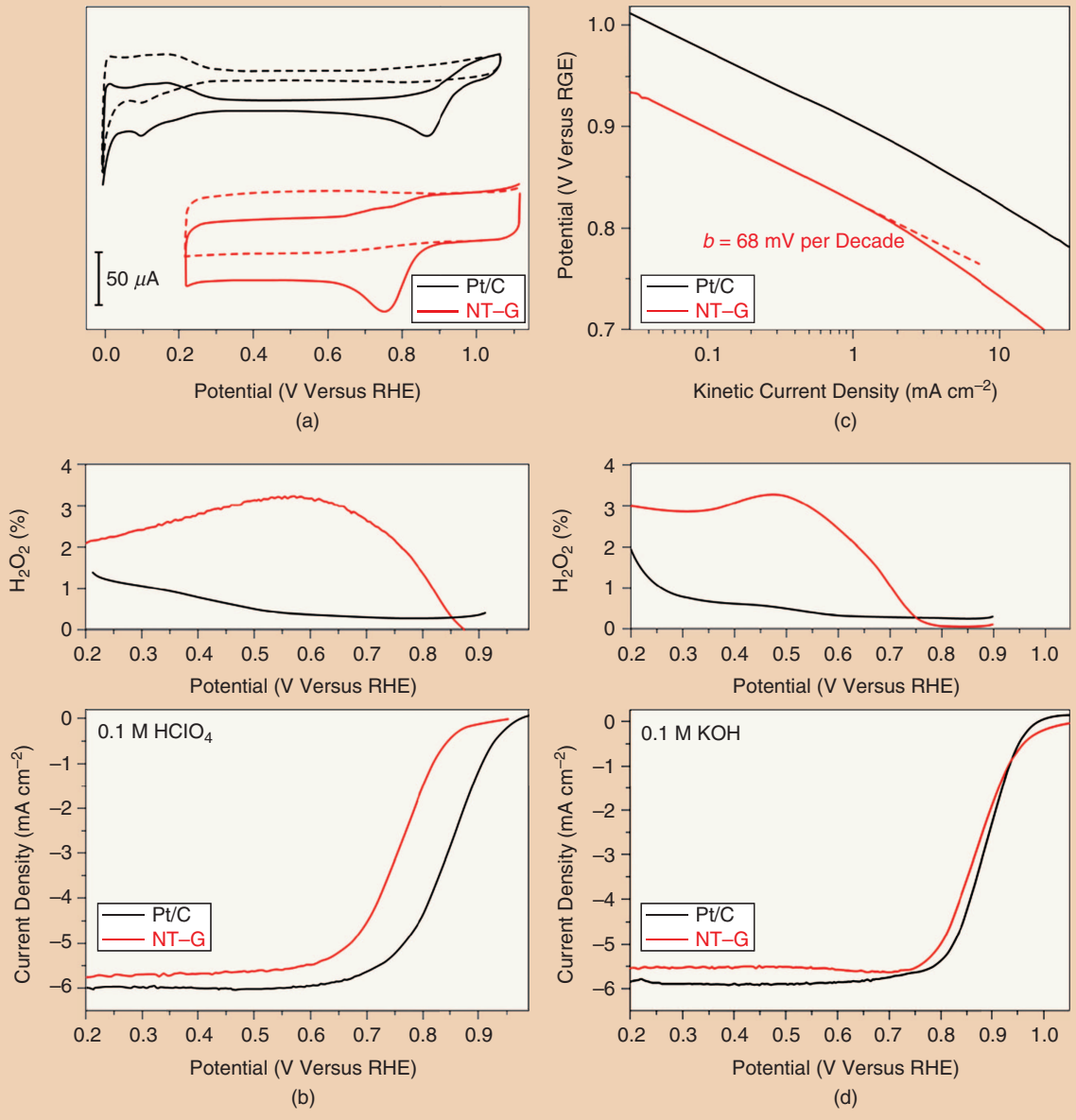


**FIGURE 16** The electrochemical characterization of the CNT-graphene ORR catalyst. (a) The cyclic voltammetry measurements of commercial 20% Pt/C (black) and CNT-graphene (NT-G) (red) catalysts in $O_2$-saturated (solid) or argon-saturated (dotted) 0.1 M $HClO_4$. (b) The rotating ring-disk electrode (RRDE) polarization curves and peroxide yield of Pt/C (black) and NT-G (red) in $O_2$-saturated 0.1 M $HClO_4$. (c) The kinetic current densities versus the potential derived from the mass transport correction of the corresponding RRDE disk currents in (b). (d) The RRDE polarization curves and peroxide yield of Pt/C (black) and NT-G (red) in $O_2$-saturated 0.1 M KOH. NT-G exhibits high ORR electrocatalytic activity in both acidic and alkaline electrolytes. For all the RRDE measurements, the loading of catalysts is 16 mgPt $cm^{-2}$ for Pt/C and 0.485 mg $cm^{-2}$ for NT-G. The electrode rotation speed, 1,600 r/min; scan rate, 5 mV $s^{-1}$. Pt data are collected from anodic sweeps. (Images from [216], used with permission.)

Successfully achieving performance and durability targets will provide enormous cost advantages to commercialization efforts of metal–air batteries.

nanofibers could be used as ORR electrocatalyst using 1-D zeolitic imidazolate framework (ZIF)-8 nanofibers as the precursors. They exhibited excellent electrocatalytic activity of an onset potential of ~–0.07 V, half-wave potential of ~–0.161 V, and long-term durability in alkaline media [225].

Zhong et al. developed graphene-based N-doped porous carbon sheets catalyst by in situ growing two-dimensional (2-D) sandwichlike ZIF on graphene oxide. It shows comparable onset potential, higher current density, and superior durability in the ORR [226].

Ma et al. designed and prepared the hybrid $Co_3O_4$-carbon porous nanowire arrays electrocatalyst by carbonization of the MOF directly grown on copper (Cu) foil under an $N_2$ atmosphere. It affords the current density of 10 mA $cm^{-2}$ at 1.52 V, better than that of $IrO_2/C$ and most of the Co-based transition-metal electrocatalysts during OER process [227].

Xia et al. reported the direct synthesis of N-doped CNT frameworks derived from ZIF-67 as an active and stable bifunctional electrocatalyst, as shown in Figure 18. The exceptional electrocatalytic activity might be mainly attributed to chemical compositions and the robust hollow structure composed of interconnected crystalline N-doped CNTs [228].

## METAL-FREE MATERIALS

Successfully achieving performance and durability targets will provide enormous cost advantages to commercialization efforts of metal–air batteries [85], [91]. As an alternative strategy, metal-free catalysts, such as conducting polymers and carbon-based materials, greatly promote the design and screening of nonprecious electrocatalysts.

The heterocyclic conducting polymers, such as poly(3,4-ethylenedioxythiophene) (PEDOT), polypyrrole (PPy), and PANI, have been intensively investigated in oxygen electrochemistry due to their low cost, high electrical

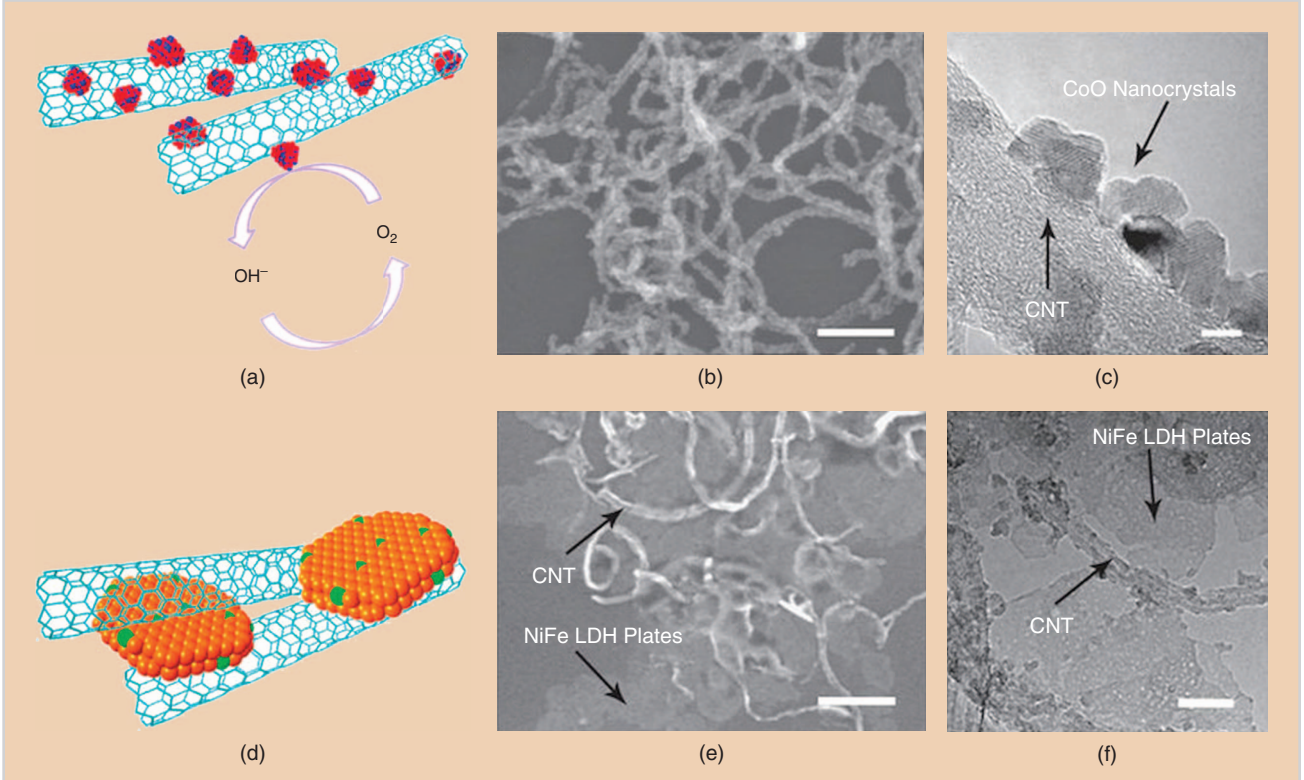


**FIGURE 17** The ORR and OER electrocatalysis. Strongly coupled inorganic/CNT hybrids for ORR and OER electrocatalysis with low overpotentials. (a)–(c) The schematic structure, SEM, and TEM images of the CoO/N-CNT hybrid. (d)–(f) The schematic structure, SEM, and TEM images of the NiFe-LDH/CNT hybrid. The scale bars are 200, 5, 200, and 20 nm, respectively, in (b), (c), (e), and (f). (Images and photos courtesy of Macmillan Publishers Limited.)

conductivity, and abundant function [212], [229]. Winther-Jensen et al. developed an air electrode coated with PEDOT in a Zn–air battery, as shown in Figure 19. The PEDOT that acts as the electrocatalyst for OER exhibits respectable durability, as it could continuously operate for 1,500 h without material degradation or deterioration in performance [230]. PPy with the character of high conductivity and hydrophilic properties could be used as the support and catalysts for the cathode of nonaqueous Li–air batteries. Cui et al. designed the nano-PPy tubes cathode with tubular morpholoy, and its abundant gas diffusion channels and reaction space greatly improved the capacity, cycling stability, and especially the rate performance of the batteries [231].

PANI is a conducting polymer with the structure of conjugated aromatic rings connected via nitrogen-containing groups that is similar to graphite. The pyrolysis of PANI could facilitate the integration of N-containing active sites into the carbon matrix [231]. Zhang et al. reported the pyrolysis of PANI aerogels method to obtain a three-dimensional (3-D) N and P codoped mesoporous nanocarbon (NPMC) foam whose precursor was prepared from a template-free polymerization of aniline in the presence of phytic acid (Figure 20). The NPMCs that act as metal-free bifunctional electrocatalysts for ORR and OER in a primary Zn–air battery show good stability of 600 cycles for 100 h of operation. Furthermore, they exhibit an open-circuit potential (OCP) of 1.48 V, a specific capacity of 735 mAhg $Zn^{-1}$, a peak power density of 55 mW $cm^{-2}$, and stable operation for 240 h after mechanical recharging [232].

> Graphene and functionalized graphene as novel ultrathin 2-D carbon materials have received a great deal of attention as metal-free electrocatalysts.

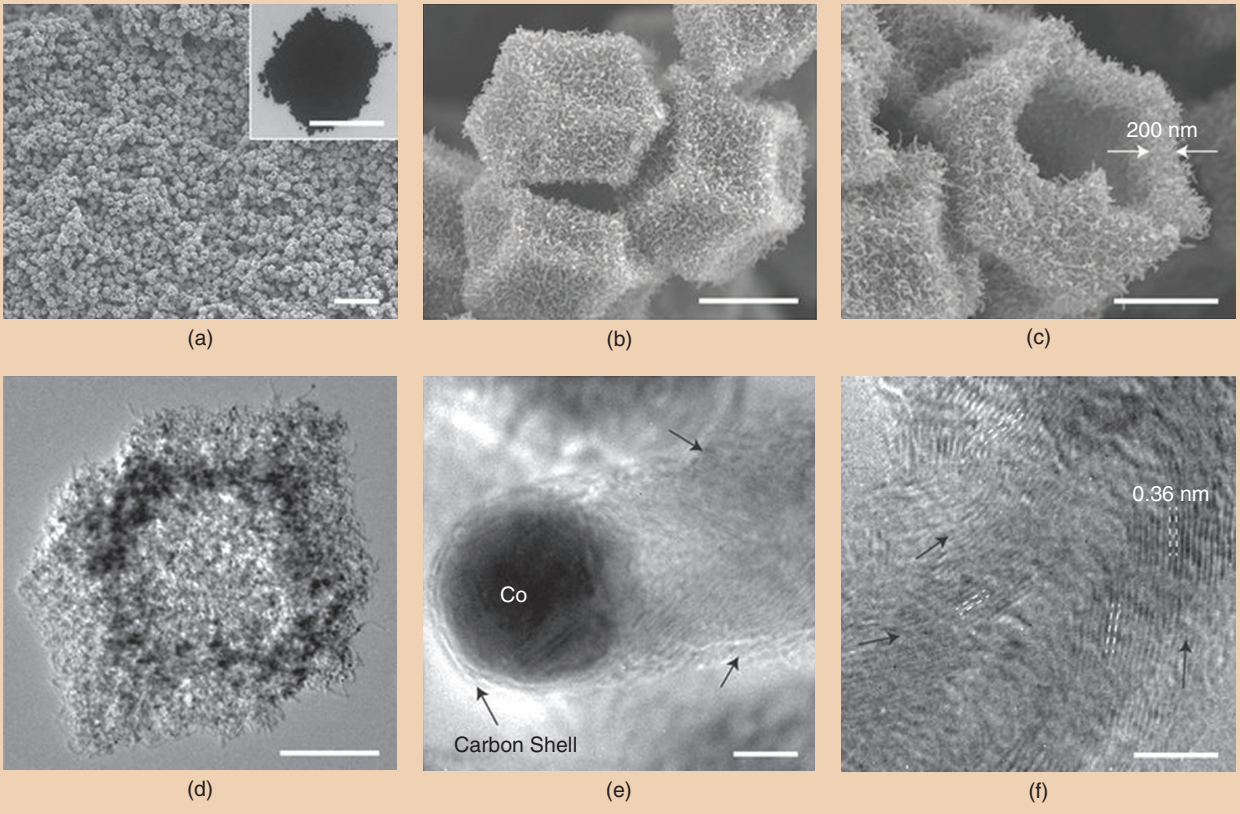


**FIGURE 18** The morphology and structural characterization of N-doped CNT frameworks obtained at 700 °C in the presence of $H_2$. (a)–(c) Field-emission scanning electron microscope images. (d) A TEM image. (e) and (f) High-resolution transmission electron microscopy (HRTEM) images. In (f), 0.36 nm refers to the lattice spacing indicated by the white dashed lines on the carbon (002) plane. The arrows in (e) and (f) indicate the direction of the graphitic layers. The inset of (a) is a digital photo, and the scale bar is 1 cm. The other scale bars are (a) 10 $\mu$m, (b) and (c) 1 $\mu$m, (d) 500 nm, and (e) and (f) 5 nm. (Photos courtesy of Macmillan Publishers Limited.)

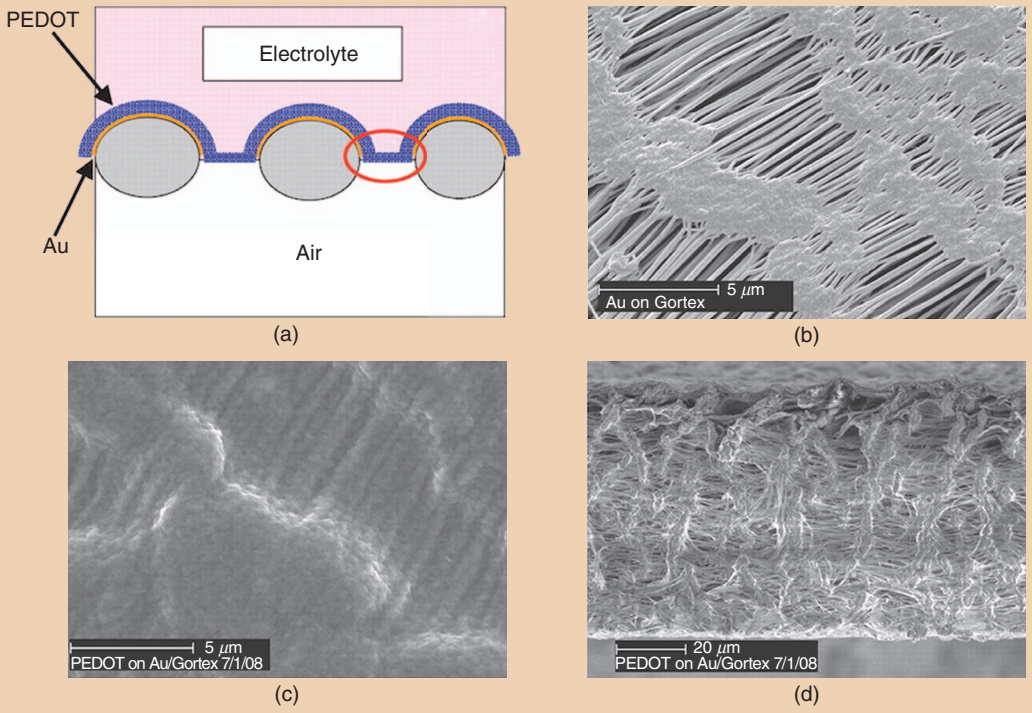


**FIGURE 19** (a) A schematic representation of the PEDOT/Goretex air electrode. (b)–(d) SEM images. (b) The Goretex membrane coated with gold (Au). The scale bar is 5 mm. (c) The PEDOT/Goretex structure. The scale bar is 5 mm. (d) The cross section of the electrode with thickness measurements of the PEDOT layer. The scale bar is 20 mm. (Image and photos courtesy of American Association for the Advancement of Science.)

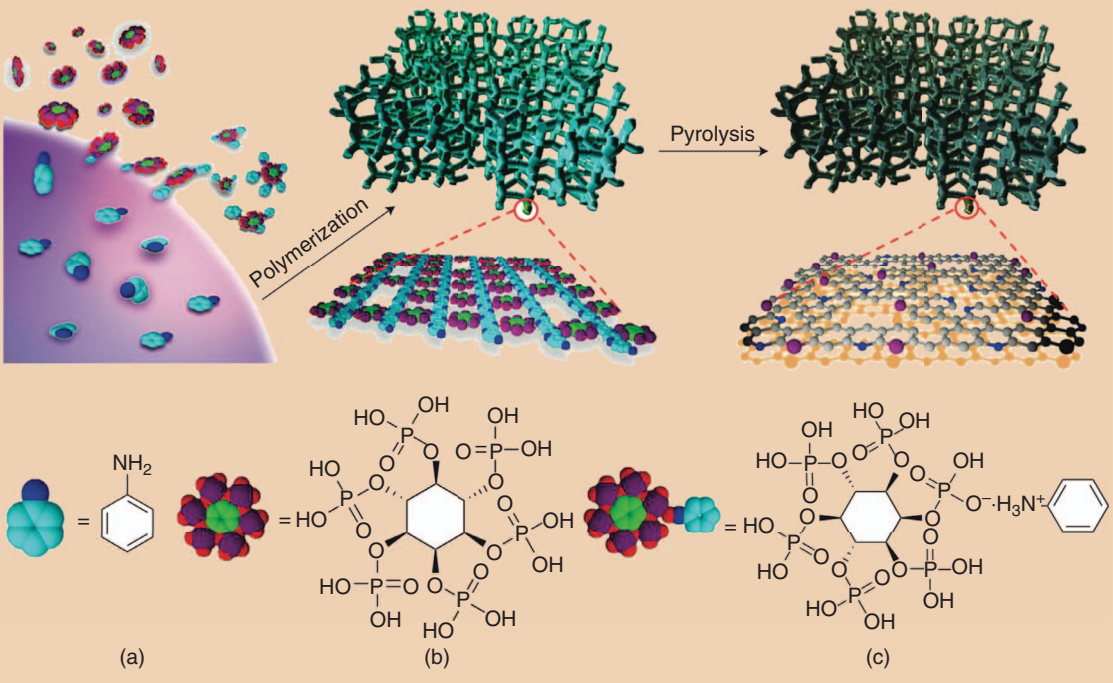


**FIGURE 20** The preparation of the NPMC electrocatalysts. (a) A schematic illustration of the preparation process for the NPMC foams. (a) An aniline (b) phytic acid (c) complex s formed (for clarity, only one of the complexed anilines is shown for an individual phytic acid), followed by oxidative polymerization into a 3-D PANI hydrogel crosslinked with phytic acids. As each phytic acid molecule can complex with up to six aniline monomers, phytic acid can be used as the crosslinker and protonic dopant to directly form the 3-D PANI hydrogel network; for clarity, only a piece of the 2-D network building block is shown in the enlarged view under the 3-D PANI hydrogel. The PANI hydrogel is freeze-dried into an aerogel and pyrolysed in Ar to produce the NPMC (for clarity, only a piece of the 2-D NPMC network building block is shown in the enlarged view under the 3-D NPMC). (Image courtesy of Macmillan Publishers Limited.)

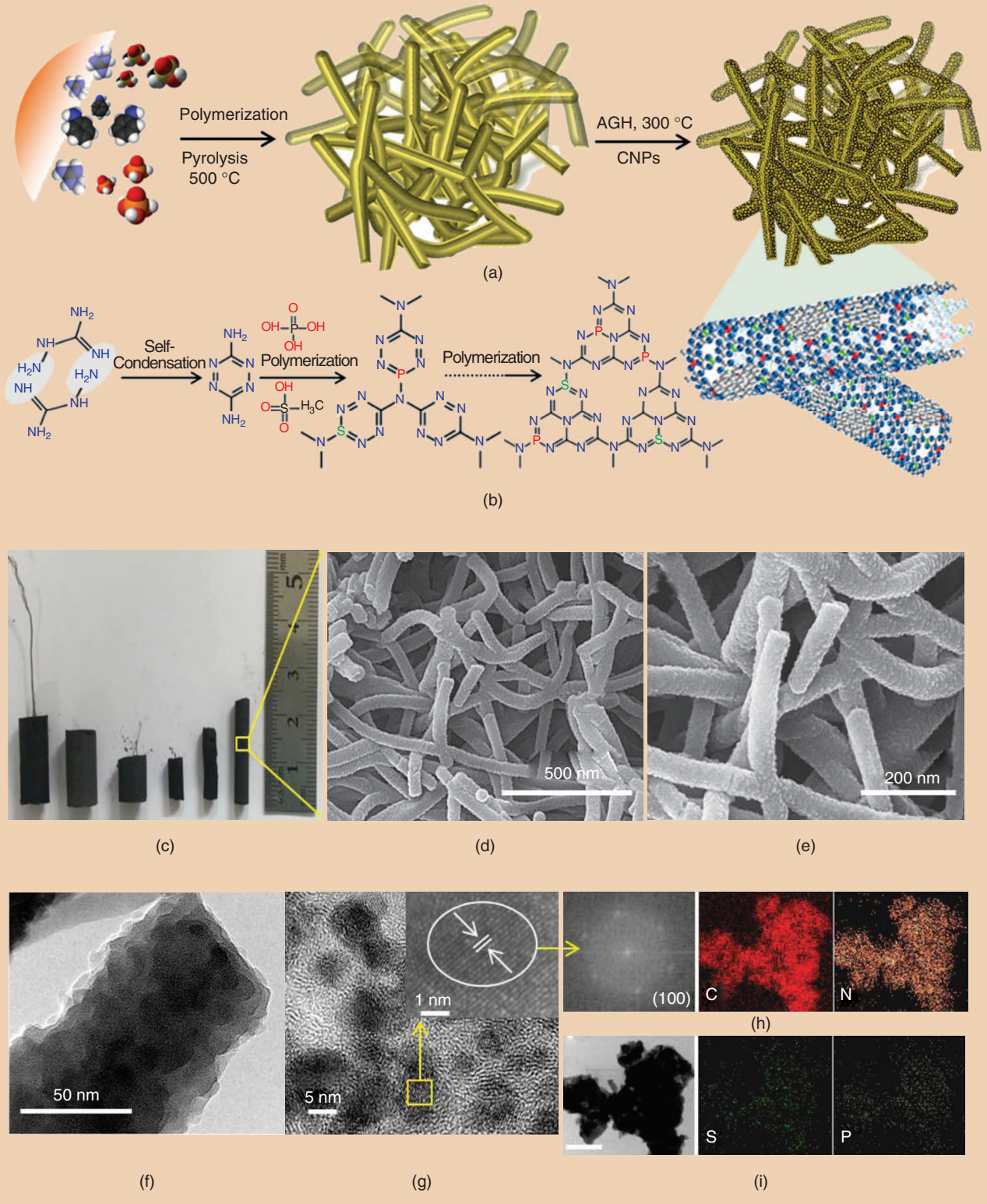


**FIGURE 21** (a) The schematics showing the synthesis of P, S-CNS catalysts and (b) the reaction mechanism for the formation of the C-N polymeric complex. (c) A photograph of as-synthesized cylindrical spongelike P, S-CNS structure. (d) and (e) SEM, (f) TEM, and (g) HRTEM images of P, S-CNS catalyst [the inset in (g) shows an enlarged view]. (h) A corresponding fast Fourier transform (FFT) pattern of the crystallite in the inset of (g). (i) The TEM and the elemental maps of C, N, P, and S of P, S-CNS. The scale bar is 300 nm. AGH: aminoguanidine hydrochloride; CNPs: carbon nanoparticles. (Images and photos courtesy of American Chemical Society.)

Besides the compounds, a fully organic N(5)-ethylflavinium ion was found to function as an OER electrocatalyst with a high overpotential of –0.73 V (versus SHE) [233].

The traditional carbon materials applied as catalysts in Li–air batteries were investigated in early work [234]–[237]. Zhao et al. found that nitrogen-doped graphite nanomaterials exhibit highly efficient OER activity in alkaline media exceeding those of traditional electrocatalysts. They generate a current density of 10 mA $cm^{-2}$ at the overpotential of 0.38 V [238]. Shinde et al. reported a scalable strategy for the fabrication of a 3-D carbon nanoparticle sandwiched P and S codoped carbon nitride sponge (P, S-CNS) by polymerization of aminoguanidine (Figure 21). It shows outstanding bifunctional electrocatalytic performance of the ORR and OER and superior stability over 500 cycles in rechargeable Zn–air batteries [239].

CNT, one of the most important carbon-based materials, has been widely explored as the electrocatalyst for ORR and OER. Its use as the metal/metal oxides-catalyst support has been previously demonstrated. The metal-free CNT with doping creates net charges on carbon atoms, thus showing ORR activities [240]. Gong et al. first reported the vertically aligned (VA) N-doped CNT could be applied as the metal-free ORR catalyst. The superb performance shows a steady-state output potential of –80 mV and a current density of 4.1 mA $cm^{-2}$ at –0.22 V [241]. Furthermore, CNTs containing both B and N atoms (BCN nanotube) are attractive materials as electrocatalysts because the band gap can be tunable [242], [243]. Wang et al. demonstrated that VA-BCN nanotube shows the highest ORR activities among the VA-CNT, B-doped VA-CNT (VA-BCNT), and N-doped VA-CNT (VA-NCNT), such as its more positive half-wave potential of 0.25 V, and the higher diffusion current density as well as the kinetic current density (Figure 22) [240].

Graphene and functionalized graphene as novel ultrathin 2-D carbon materials have received a great deal of attention as metal-free electrocatalysts [244], [245]. Many achievements of graphene-based metal-free electrocatalysts for metal–air batteries have been obtained by heteroatom doping [246]–[248]. Yang et al. designed a 3-D graphene nanoribbon network with the doping of nitrogen (N-GRW), and further experiments identified that the electrodonating quaternary N sites and the electron-withdrawing pyridinic N moieties were responsible for ORR and OER, respectively. The assembled Zn–air battery with the N-doped graphene-based air electrode shows an OCP of 1.46 V, a peak power density of 65 mW $cm^{-2}$, a specific capacity of 873 mAh $g^{-1}$, and excellent charge/discharge cycling stability, as shown in Figure 23 [249].

A more complex active site of Cu(I)-N within graphene-based air electrode in a Zn–air battery was identified by the Cu-K edge X-ray absorption near edge structure spectra and the extended X-ray absorption fine-structure spectroscopy. Furthermore, it shows the current density of 142 mA $cm^{-2}$ at 1.0 V and the peak power density of 210 mW $cm^{-2}$ with an extreme low catalyst loading of 0.4 mg $cm^{-2}$ [250]. To fully exploit the high-performance electrocalyst, graphene integrated with CNTs was demonstrated as an effective way because it could prevent the stacking [251]. By using this strategy, Yang

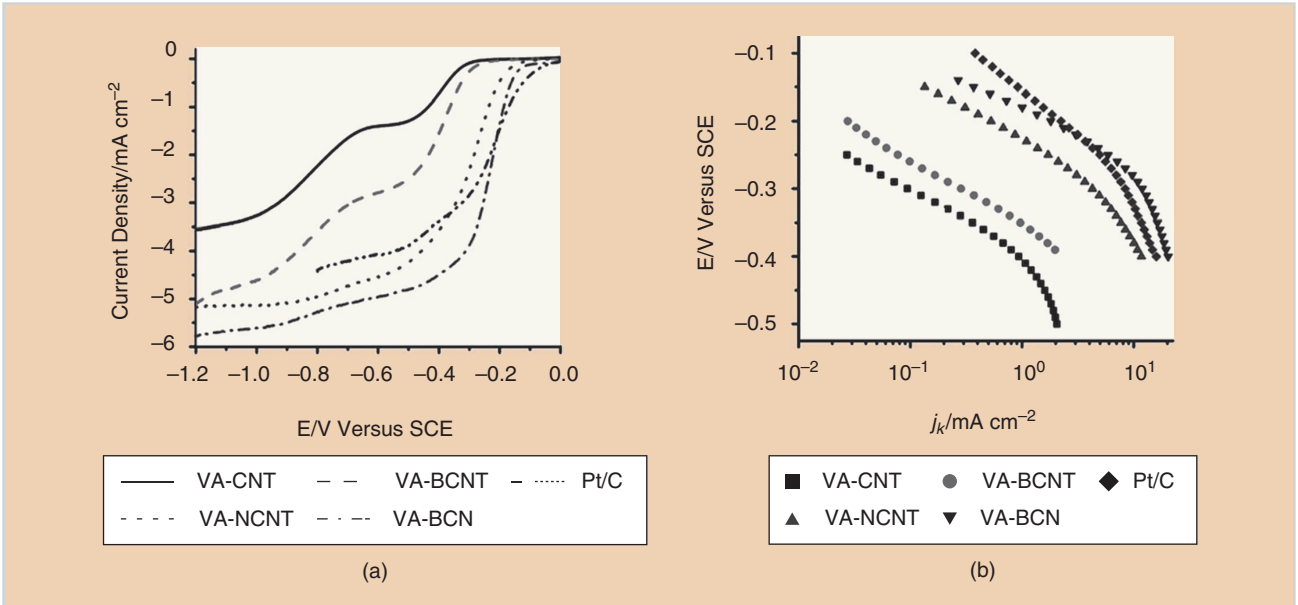


**FIGURE 22** (a) The linear-sweep voltammetry curves of various electrodes in an oxygen-saturated 0.1 M KOH electrolyte at a scan rate of 10 mV/s and a rotation rate of 1,000 r/min. (b) Tafel plots are derived from Figure 3(a) in the low-current region. (Figure courtesy of WILEY-VCH Verlag GmbH and Co. KGaA, Weinheim.)

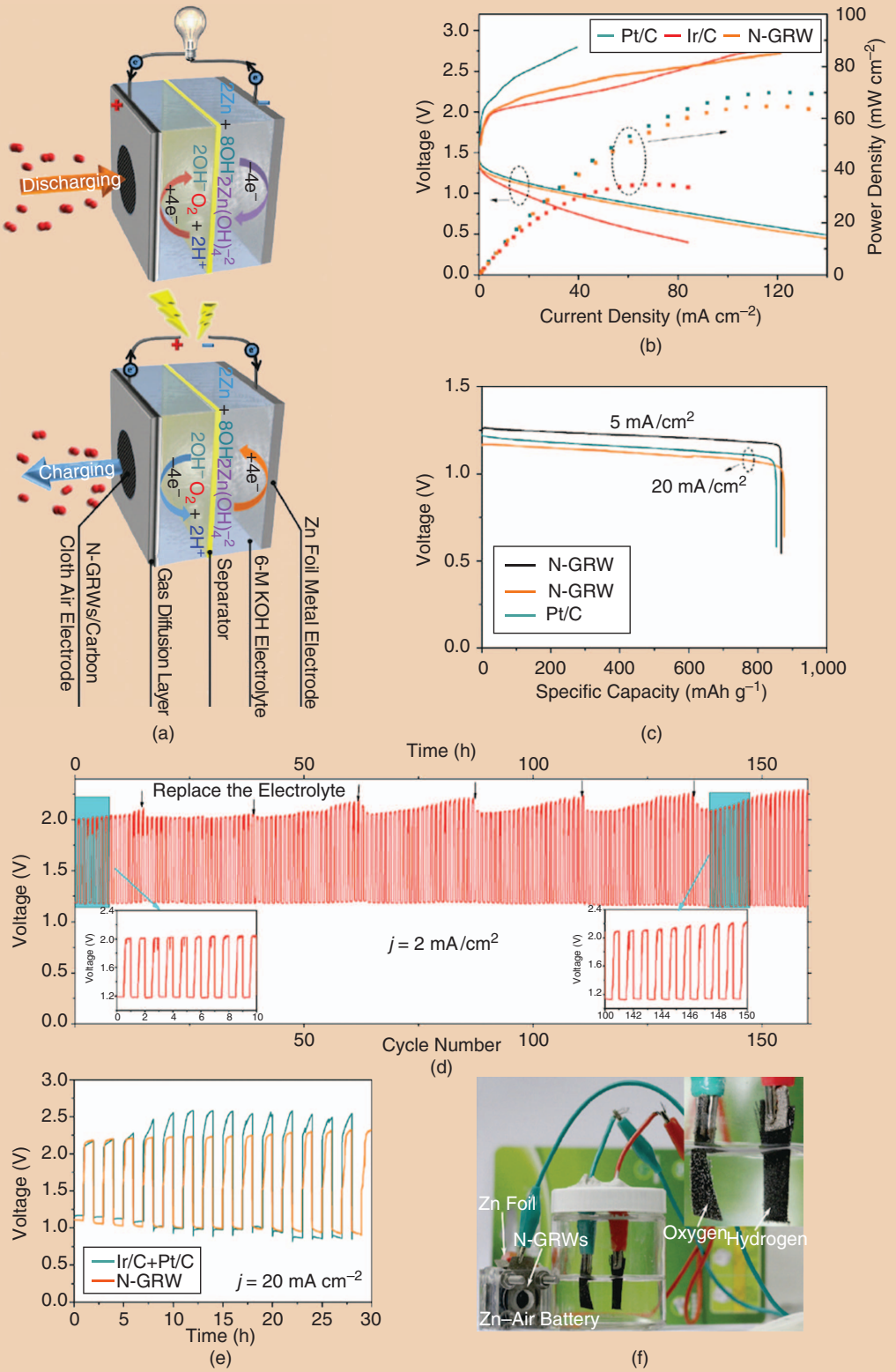


**FIGURE 23** The application of N-GRW bifunctional catalyst in rechargeable Zn–air batteries. (a) The schematic of a Zn–air battery at charging and discharging conditions. (b) Galvanodynamic charge/discharge profiles and power density curves of Zn–air batteries assembled from the N-GRW, Pt/C, Ir/C, and mixed Pt/C + Ir/C (1:1 by weight) air electrode. (c) Discharge curves of Zn–air batteries assembled from the N-GRW and Pt/C catalysts at 5-and 20-mA $cm^{-2}$ discharging rate. (d) Charging/discharging cycling at a current density of 2 mA $cm^{-2}$. Insets show the initial and after a long time cycling testing charging/discharging curves of a Zn–air battery assembled from N-GRW as an air catalyst. (e) Charging/discharging cycling curves of Zn–air batteries assembled from the N-GRW (yellow line) and mixed Pt/C + Ir/C air electrode (blue line) at a current density of 20 mA $cm^{-2}$ (catalyst loading amount: 0.5 mg $cm^{-2}$ for mixed Pt/C + Ir/C). (f) An electrolysis cell powered by a Zn–air battery. The inset shows the bubble formation on both cathode and anode electrodes. All Zn–air batteries were tested in air at room temperature (catalyst loading amount: 0.5 mg $cm^{-2}$ for all Zn–air batteries). (Images and photo courtesy of American Association for the Advancement of Science.)

Li–air and Zn–air batteries with high specific energy densities hold promise as the next-generation battery technologies.

et al. confirmed the specific surface area and electric conductivity of N, P codoped graphene/CNTs could be significantly increased, and thus an excellent performance of Zn–air battery with the specific capacity of 684 mAh $g^{-1}$ was obtained [252].

## SUMMARY AND OUTLOOK

In this article, we summarized the recent progress in nonprecious catalysts for Li–air and Zn–air batteries. The electrocatalysts ranging from transition-metal oxides and inorganic–organic hybrid materials to metal-free materials were discussed with the demonstration of synthetic methods, electrocatalytic mechanism, and performance. Transition-metal oxides, in particular, Mn-based oxides, mixed Ni-Fe or Ni-Co oxides, and perovskites, have been intensely investigated both in ORR and OER because of their high activity and durability in alkaline electrolytes. The catalytic performance could be tuned through morphology, structure, composition, transition-metal valence, and innovative synthetic strategy.

Some fundamental understanding of the catalytic mechanism was also discussed. Inorganic–organic hybrid materials with higher conductivity than that of transition-metal oxides have attracted much attention. To improve the activity and stability of these materials, heat treatment has been a widely used method. Beyond that, integration of carbon materials with active metal oxide or nitrides to form hybrid materials is attracting more interest.

MOFs highlight promising electrocatalysts in Li–air and Zn–air batteries because of their high specific surface area and various architectures. Metal-free electrocatalysts, including conducting polymers, CNTs, and graphene-based carbon materials, appear to be the rising types of electrocatalytic materials in Li–air and Zn–air batteries. Heteroatom doping has been demonstrated as an effective way to improve the catalytic performance through tuning the active sites, electronic structure, and defects. We also briefly introduced the background of Li–air and Zn–air batteries, and some electrocatalytic mechanisms of ORR and OER are mentioned.

Li–air and Zn–air batteries with high specific energy densities hold promise as the next-generation battery technologies. The electrocatalysts play a key role in realizing that potential. Some points for developing high-performance nonprecious catalysts are the following:

1) The precise microstructural control of electrocatalysts (e.g., 2-D graphene and MOFs) for exposing more active sites and obtaining high specific surface area still needs more investigation.
2) The design of special structure and morphology of hybrid or metal-free materials are beneficial in understanding and improving the catalytic activity and battery performance.
3) More fundamental understanding of the electrocatalytic mechanisms of ORR and OER in carbon-based electrocatalysts through advanced characterization technologies and theoretical investigations is needed.

## ACKNOWLEDGMENTS

The corresponding authors for this article are Rui Cai and Zhongwei Chen.

## ABOUT THE AUTHORS

***Tongwen Yu*** (t83yu@uwaterloo.ca) is with the Department of Chemical Engineering, Waterloo Institute for Nanotechnology, Waterloo Institute for Sustainable Energy, University of Waterloo, Ontario, Canada.

***Jing Fu*** (j42fu@uwaterloo.ca) is with the Department of Chemical Engineering, Waterloo Institute for Nanotechnology, Waterloo Institute for Sustainable Energy, University of Waterloo, Ontario, Canada.

***Rui Cai*** (cairui@dicp.ac.cn) is with the State Key Laboratory of Catalysis, Dalian Institute of Chemical Physics, Chinese Academy of Sciences, Dalian, China.

***Aiping Yu*** (aipingyu@uwaterloo.ca) is with the Department of Chemical Engineering, Waterloo Institute for Nanotechnology, Waterloo Institute for Sustainable Energy, University of Waterloo, Ontario, Canada.

***Zhongwei Chen*** (zhwchen@uwaterloo.ca) is with the Department of Chemical Engineering, Waterloo Institute for Nanotechnology, Waterloo Institute for Sustainable Energy, University of Waterloo, Ontario, Canada.

## REFERENCES

[1] MIT Energy Initiative. (2015). Appendix C—Energy storage systems for the electric power sector in the future of solar energy: An interdisciplinary MIT study Masssachusetts Institute of Technology. Cambridge, MA. [Online]. Available: http://mitei.mit.edu/futureofsolar

[2] P. G. Bruce, S. A. Freunberger, L. J. Hardwick, and J.-M. Tarascon, "Li-O2 and Li-S batteries with high energy storage," *Nature Mater.*, vol. 11, no. 1, pp. 19–29, 2012.

[3] J. S. Lee, S. Tai Kim, R. Cao, N. S. Choi, M. Liu, K. T. Lee, and J. Cho, "Metal–air batteries with high energy density: Li–air versus Zn–air," *Adv. Energy Mater.*, vol. 1, no. 1, pp. 34–50, 2011.

[4] F. Beck and P. Rüetschi, "Rechargeable batteries with aqueous electrolytes," *Electrochim. Acta*, vol. 45, no. 15, pp. 2467–2482, 2000.

[5] K. F. Blurton and A. F. Sammells, "Metal/air batteries: Their status and potential—a review," *J. Power Sources*, vol. 4, no. 4, pp. 263–279, 1979.

[6] F. Cheng and J. Chen, "Metal–air batteries: From oxygen reduction electrochemistry to cathode catalysts," *Chem. Soc. Rev.*, vol. 41, no. 6, pp. 2172–2192, 2012.

[7] Z.-L. Wang, D. Xu, J.-J. Xu, and X.-B. Zhang, "Oxygen electrocatalysts in metal–air batteries: From aqueous to nonaqueous electrolytes," *Chem. Soc. Rev.*, vol. 43, no. 22, pp. 7746–7786, 2014.

[8] M. D. Radin and D. J. Siegel, "Non-aqueous metal–oxygen batteries: Past, present, and future," in *Rechargeable Batteries Materials, Technologies and New Trends*, Z.-C. Zhang, and S.-S. Zhang, Eds. Cham, Switzerland: Springer, 2015, pp. 511–539.

[9] B. Peng and J. Chen, "Functional materials with high-efficiency energy storage and conversion for batteries and fuel cells," *Coord. Chem. Rev.*, vol. 253, no. 23, pp. 2805–2813, 2009.

[10] J.-G. Zhang, P. G. Bruce, and X. G. Zhang, "Metal–air batteries," in *Handbook of Battery Materials*, C. Daniel and J.-O. Besenhard, Eds. Weinheim, Germany: Wiley-VCH Verlag GmbH & Co., 2011, pp. 757–795.

[11] K. Abraham and Z. Jiang, "A polymer electrolyte-based rechargeable lithium/oxygen battery," *J. Electrochem. Soc.*, vol. 143, no. 1, pp. 1–5, 1996.

[12] T. Ogasawara, A. Débart, M. Holzapfel, P. Novák, and P. G. Bruce, "Rechargeable Li2O2 electrode for lithium batteries," *J. Am. Chem. Soc.*, vol. 128, no. 4, pp. 1390–1393, 2006.

[13] G. Girishkumar, B. McCloskey, A. Luntz, S. Swanson, and W. Wilcke, "Lithium–air battery: Promise and challenges," *J. Phys. Chem. Lett.*, vol. 1, no. 14, pp. 2193–2203, 2010.

[14] B. D. Adams, C. Radtke, R. Black, M. L. Trudeau, K. Zaghib, and L. F. Nazar, "Current density dependence of peroxide formation in the Li–O 2 battery and its effect on charge," *Energy Environ. Sci.*, vol. 6, no. 6, pp. 1772–1778, 2013.

[15] R. R. Mitchell, B. M. Gallant, Y. Shao-Horn, and C. V. Thompson, "Mechanisms of morphological evolution of Li2O2 particles during electrochemical growth," *J. Phys. Chem. Lett.*, vol. 4, no. 7, pp. 1060–1064, 2013.

[16] S. A. Freunberger, Y. Chen, Z. Peng, J. M. Griffin, L. J. Hardwick, F. Bardé, P. Novák, and P. G. Bruce, "Reactions in the rechargeable lithium–O2 battery with alkyl carbonate electrolytes," *J. Am. Chem. Soc.*, vol. 133, no. 20, pp. 8040–8047, 2011.

[17] S. A. Freunberger, Y. Chen, N. E. Drewett, L. J. Hardwick, F. Bardé, and P. G. Bruce, "The lithium–oxygen battery with ether-based electrolytes," *Angew. Chem. Int. Ed.*, vol. 50, no. 37, pp. 8609–8613, 2011.

[18] M. Park, H. Sun, H. Lee, J. Lee, and J. Cho, "Lithium–air batteries: Survey on the current status and perspectives towards automotive applications from a battery industry standpoint," *Adv. Energy Mater.*, vol. 2, no. 7, pp. 780–800, 2012.

[19] Y. Shao, F. Ding, J. Xiao, J. Zhang, W. Xu, S. Park, J. G. Zhang, Y. Wang, and J. Liu, "Making Li–air batteries rechargeable: Material challenges," *Adv. Funct. Mater.*, vol. 23, no. 8, pp. 987–1004, 2013.

[20] D. Aurbach, M. Daroux, P. Faguy, and E. Yeager, "The electrochemistry of noble metal electrodes in aprotic organic solvents containing lithium salts," *J. Electroanal. Chem. Interfacial Electrochem.*, vol. 297, no. 1, pp. 225–244, 1991.

[21] W. Xu, K. Xu, V. V. Viswanathan, S. A. Towne, J. S. Hardy, J. Xiao, Z. Nie, D. Hu, D. Wang, and J.-G. Zhang, "Reaction mechanisms for the limited reversibility of Li–O2 chemistry in organic carbonate electrolytes," *J. Power Sources*, vol. 196, no. 22, pp. 9631–9639, 2011.

[22] W. Xu, V. V. Viswanathan, D. Wang, S. A. Towne, J. Xiao, Z. Nie, D. Hu, and J.-G. Zhang, "Investigation on the charging process of Li2 O2-based air electrodes in Li–O2 batteries with organic carbonate electrolytes," *J. Power Sources*, vol. 196, no. 8, pp. 3894–3899, 2011.

[23] B. McCloskey, D. Bethune, R. Shelby, G. Girishkumar, and A. Luntz, "Solvents' critical role in nonaqueous lithium–oxygen battery electrochemistry," *J. Phys. Chem. Lett.*, vol. 2, no. 10, pp. 1161–1166, 2011.

[24] V. S. Bryantsev, V. Giordani, W. Walker, M. Blanco, S. Zecevic, K. Sasaki, J. Uddin, D. Addison, and G. V. Chase, "Predicting solvent stability in aprotic electrolyte Li–air batteries: nucleophilic substitution by the superoxide anion radical (O2•–)," *J. Phys. Chem. A*, vol. 115, no. 44, pp. 12,399–12,409, 2011.

[25] V. S. Bryantsev and M. Blanco, "Computational study of the mechanisms of superoxide-induced decomposition of organic carbonate-based electrolytes," *J. Phys. Chem. Lett.*, vol. 2, no. 5, pp. 379–383, 2011.

[26] Z. Peng, S. A. Freunberger, L. J. Hardwick, Y. Chen, V. Giordani, F. Bardé, P. Novák, D. Graham, J. M. Tarascon, and P. G. Bruce, "Oxygen reactions in a non-aqueous Li+ electrolyte," *Angew. Chem. Int. Ed.*, vol. 123, no. 28, pp. 6475–6479, 2011.

[27] C. O. Laoire, S. Mukerjee, K. M. Abraham, E. J. Plichta, and M. A. Hendrickson, "Elucidating the mechanism of oxygen reduction for lithium–air battery applications," *J. Phys. Chem. C*, vol. 113, no. 46, pp. 20127–20134, 2009.

[28] C. O. Laoire, S. Mukerjee, K. Abraham, E. J. Plichta, and M. A. Hendrickson, "Influence of nonaqueous solvents on the electrochemistry of oxygen in the rechargeable lithium–air battery," *J. Phys. Chem. C*, vol. 114, no. 19, pp. 9178–9186, 2010.

[29] A. Garsuch, D. M. Badine, K. Leitner, L. H. Gasparotto, N. Borisenko, F. Endres, M. Vracar, J. Janek, and R. Oesten, "Investigation of various ionic liquids and catalyst materials for lithium–oxygen batteries," *Z. Phys. Chem.*, vol. 226, no. 2, pp. 107–119, 2012.

[30] C. J. Allen, S. Mukerjee, E. J. Plichta, M. A. Hendrickson, and K. Abraham, "Oxygen electrode rechargeability in an ionic liquid for the Li–air battery," *J. Phys. Chem. Lett.*, vol. 2, no. 19, pp. 2420–2424, 2011.

[31] F. De Giorgio, F. Soavi, and M. Mastragostino, "Effect of lithium ions on oxygen reduction in ionic liquid-based electrolytes," *Electrochem. Commun.*, vol. 13, no. 10, pp. 1090–1093, 2011.

[32] F. Mizuno, S. Nakanishi, A. Shirasawa, K. Takechi, T. Shiga, H. Nishikoori, and H. Iba, "Design of non-aqueous liquid electrolytes for rechargeable Li-O 2 batteries," *Electrochem.*, vol. 79, no. 11, pp. 876–881, 2011.

[33] G. H. Lane, P. M. Bayley, B. R. Clare, A. S. Best, D. R. MacFarlane, M. Forsyth, and A. F. Hollenkamp, "Ionic liquid electrolyte for lithium metal batteries: Physical, electrochemical, and interfacial studies of N-Methyl-N-butylmorpholinium Bis (fluorosulfonyl) imide," *J. Phys. Chem. C*, vol. 114, no. 49, pp. 21,775–21,785, 2010.

[34] I. Osada, H. de Vries, B. Scrosati, and S. Passerini, "Ionic–liquid–based polymer electrolytes for battery applications," *Angew. Chem. Int. Ed.*, vol. 55, pp. 500–513, 2016.

[35] Y. Wang, P. He, and H. Zhou, "A lithium–air capacitor–battery based on a hybrid electrolyte," *Energy Environ. Sci.*, vol. 4, no. 12, pp. 4994–4999, 2011.

[36] S. Hasegawa, N. Imanishi, T. Zhang, J. Xie, A. Hirano, Y. Takeda, and O. Yamamoto, "Study on lithium/air secondary batteries—stability of NASICON-type lithium ion conducting glass–ceramics with water," *J. Power Sources*, vol. 189, no. 1, pp. 371–377, 2009.

[37] T. Zhang, N. Imanishi, S. Hasegawa, A. Hirano, J. Xie, Y. Takeda, O. Yamamoto, and N. Sammes, "Li/polymer electrolyte/water stable lithium-conducting glass ceramics composite for lithium–air secondary batteries with an aqueous electrolyte," *J. Electrochem. Soc.*, vol. 155, no. 12, pp. A965–A969, 2008.

[38] T. Zhang, N. Imanishi, Y. Shimonishi, A. Hirano, J. Xie, Y. Takeda, O. Yamamoto, and N. Sammes, "Stability of a water-stable lithium metal anode for a lithium–air battery with acetic acid–water solutions," *J. Electrochem. Soc.*, vol. 157, no. 2, pp. A214–A218, 2010.

[39] T. Zhang, N. Imanishi, S. Hasegawa, A. Hirano, J. Xie, Y. Takeda, O. Yamamoto, and N. Sammes, "Water-stable lithium anode with the three-layer construction for aqueous lithium–air secondary batteries," *Electrochem. Solid-State Lett.*, vol. 12, no. 7, pp. A132–A135, 2009.

[40] Y. Shimonishi, T. Zhang, P. Johnson, N. Imanishi, A. Hirano, Y. Takeda, O. Yamamoto, and N. Sammes, "A study on lithium/air secondary batteries—stability of NASICON-type glass ceramics in acid solutions," *J. Power Sources*, vol. 195, no. 18, pp. 6187–6191, 2010.

[41] Y. Hou, X. Wang, Y. Zhu, C. Hu, Z. Chang, Y. Wu, and R. Holze, "Macroporous LiFePO 4 as a cathode for an aqueous rechargeable lithium battery of high energy density," *J. Mater. Chem. A*, vol. 1, no. 46, pp. 14713–14718, 2013.

[42] S. Duluard, A. Paillassa, L. Puech, P. Vinatier, V. Turq, P. Rozier, P. Lenormand, P.-L. Taberna, P. Simon, and F. Ansart, "Lithium conducting solid electrolyte Li 1.3 Al 0.3 Ti 1.7 (PO 4) 3 obtained via solution chemistry," *J. Eur. Ceram. Soc.*, vol. 33, no. 6, pp. 1145–1153, 2013.

[43] H. S. Jadhav, M.-S. Cho, R. S. Kalubarme, J.-S. Lee, K.-N. Jung, K.-H. Shin, and C.-J. Park, "Influence of B 2 O 3 addition on the ionic conductivity of Li 1.5 Al 0.5 Ge 1.5 (PO 4) 3 glass ceramics," *J. Power Sources*, vol. 241, pp. 502–508, 2013.

[44] S. Narayanan, F. Ramezanipour, and V. Thangadurai, "Dopant concentration–porosity–Li-ion conductivity relationship in garnet-type Li5+ 2 × La3Ta2–× Y × O12 (0.05≤ × ≤ 0.75) and their stability in water and 1 M LiCl," *Inorg. Chem*, vol. 54, no. 14, pp. 6968–6977, 2015.

[45] S. J. Visco, B. D. Katz, Y. S. Nimon, and L. C. De Jonghe, "Prevents the active metal from deleterious reaction with the environment on the other (cathode) side of the impervious layer, which may include aqueous or non-aqueous liquid electrolytes (catholytes) and/or a variety electrochemically active materials, including liquid, solid and gaseous oxidizers," U.S. Patent 7 282 295. Oct. 16, 2007.

[46] B. Scrosati, K. Abraham, W. A. van Schalkwijk, and J. Hassoun, *Lithium Batteries: Advanced Technologies and Applications*. Hoboken, NJ: Wiley, 2013.

[47] P. He, Y. Wang, and H. Zhou, "A Li–air fuel cell with recycle aqueous electrolyte for improved stability," *Electrochem. Commun*, vol. 12, no. 12, pp. 1686–1689, 2010.

[48] L. J. Hardwick and P. G. Bruce, "The pursuit of rechargeable non-aqueous lithium–oxygen battery cathodes," *Curr. Opin. Solid State Mater. Sci.*, vol. 16, no. 4, pp. 178–185, 2012.

[49] Y. Wang and H. Zhou, "A lithium–air battery with a potential to continuously reduce O2 from air for delivering energy," *J. Power Sources*, vol. 195, no. 1, pp. 358–361, 2010.

[50] P. He, Y. Wang, and H. Zhou, "The effect of alkalinity and temperature on the performance of lithium–air fuel cell with hybrid electrolytes," *J. Power Sources*, vol. 196, no. 13, pp. 5611–5616, 2011.

[51] Y. Wang and H. Zhou, "A lithium–air fuel cell using copper to catalyze oxygen-reduction based on copper-corrosion mechanism," *Chem. Commun.*, vol. 46, no. 34, pp. 6305–6307, 2010.

[52] A. Manthiram and L. Li, "Hybrid and aqueous lithium–air batteries," *Adv. Energy Mater.*, vol. 5, no. 4, 2015.

[53] P. Hartmann, T. Leichtweiss, M. R. Busche, M. Schneider, M. Reich, J. Sann, P. Adelhelm, and J. R. Janek, "Degradation of NASICON-type materials in contact with lithium metal: Formation of mixed conducting interphases (MCI) on solid electrolytes," *J. Phys. Chem. C*, vol. 117, no. 41, pp. 21064–21074, 2013.

[54] F. Li, H. Kitaura, and H. Zhou, "The pursuit of rechargeable solid-state Li–air batteries," *Energy Environ. Sci.*, vol. 6, no. 8, pp. 2302–2311, 2013.

[55] Y. Xu, Y. Zhang, Z. Guo, J. Ren, Y. Wang, and H. Peng, "Flexible, stretchable, and rechargeable fiber-shaped zinc–air battery based on cross-stacked carbon nanotube sheets," *Angew. Chem. Int. Ed.*, vol. 54, no. 51, pp. 15,390–15,394, 2015.

[56] J. Fu, D. U. Lee, F. M. Hassan, L. Yang, Z. Bai, M. G. Park, and Z. Chen, "Flexible high-energy polymer-electrolyte-based rechargeable zinc–air batteries," *Adv. Mater.*, vol. 27, no. 37, pp. 5617–5622, 2015.

[57] J. Park, M. Park, G. Nam, J. s. Lee, and J. Cho, "All-solid-state cable-type flexible zinc–air battery," *Adv. Mater.*, vol. 27, no. 8, pp. 1396–1401, 2015.

[58] Y. Li, M. Gong, Y. Liang, J. Feng, J.-E. Kim, H. Wang, G. Hong, B. Zhang, and H. Dai, "Advanced zinc–air batteries based on high-performance hybrid electrocatalysts," *Nature Commun.*, vol. 4, pp. 1805, 2013.

[59] B. Li, D. Geng, X. S. Lee, X. Ge, J. Chai, Z. Wang, J. Zhang, Z. Liu, T. A. Hor, and Y. Zong, "Eggplant-derived microporous carbon sheets: Towards mass production of efficient bifunctional oxygen electrocatalysts at low cost for rechargeable Zn–air batteries," *Chem. Commun.*, vol. 51, no. 42, pp. 8841–8844, 2015.

[60] M. Xu, D. Ivey, Z. Xie, and W. Qu, "Rechargeable Zn–air batteries: Progress in electrolyte development and cell configuration advancement," *J. Power Sources*, vol. 283, pp. 358–371, 2015.

[61] H.-W. Liang, Z.-Y. Wu, L.-F. Chen, C. Li, and S.-H. Yu, "Bacterial cellulose derived nitrogen-doped carbon nanofiber aerogel: An efficient metal-free oxygen reduction electrocatalyst for zinc–air battery," *Nano Energy*, vol. 11, pp. 366–376, 2015.

[62] X. Wu, F. Chen, N. Zhang, A. Qaseem, and R. L. Johnston, "A silver–copper metallic glass electrocatalyst with high activity and stability comparable to Pt/C for zinc–air batteries," *J. Mater. Chem. A*, vol. 4, no. 9, pp. 3527–3537, 2016.

[63] P.-C. Li, Y.-J. Chien, and C.-C. Hu, "Novel configuration of bifunctional air electrodes for rechargeable zinc–air batteries," *J. Power Sources*, vol. 313, pp. 37–45, 2016.

[64] L. Li, C. Liu, G. He, D. Fan, and A. Manthiram, "Hierarchical pore-in-pore and wire-in-wire catalysts for rechargeable Zn– and Li–air batteries with ultra-long cycle life and high cell efficiency," *Energy Environ. Sci.*, vol. 8, no. 11, pp. 3274–3282, 2015.

[65] Q. Li, R. Cao, J. Cho, and G. Wu, "Nanocarbon electrocatalysts for oxygen reduction in alkaline media for advanced energy conversion and storage," *Adv. Energy Mater.*, vol. 4, no. 6, 2014.

[66] T. Dirkse, "The behavior of the zinc electrode in alkaline solutions v. supersaturated zincate solutions," *J. Electrochem. Soc.*, vol. 128, no. 7, pp. 1412–1415, 1981.

[67] C. Cachet, B. Saidani, and R. Wiart, "The behavior of zinc electrode in alkaline electrolytes II. A kinetic analysis of anodic dissolution," *J. Electrochem. Soc.*, vol. 139, no. 3, pp. 644–654, 1992.

[68] L. David and B. R. Thomas, 2001. *Handbook of Batteries.* 3rd, McGraw-Hill, New York, 2002.

[69] F. R. McLarnon and E. J. Cairns, "The secondary alkaline zinc electrode," *J. Electrochem. Soc.*, vol. 138, no. 2, pp. 645–656, 1991.

[70] M. Liang, H. Zhou, Q. Huang, S. Hu, and W. Li, "Synergistic effect of polyethylene glycol 600 and polysorbate 20 on corrosion inhibition of zinc anode in alkaline batteries," *J. Appl. Electrochem.*, vol. 41, no. 8, pp. 991–997, 2011.

[71] H. Yang, Y. Cao, X. Ai, and L. Xiao, "Improved discharge capacity and suppressed surface passivation of zinc anode in dilute alkaline solution using surfactant additives," *J. Power Sources*, vol. 128, no. 1, pp. 97–101, 2004.

[72] J. Kan, H. Xue, and S. Mu, "Effect of inhibitors on Zn-dendrite formation for zinc-polyaniline secondary battery," *J. Power Sources*, vol. 74, no. 1, pp. 113–116, 1998.

[73] C. Lan, C. Lee, and T. Chin, "Tetra-alkyl ammonium hydroxides as inhibitors of Zn dendrite in Zn-based secondary batteries," *Electrochim. Acta*, vol. 52, no. 17, pp. 5407–5416, 2007.

[74] T. Adler, F. McLarnon, and E. Cairns, "Low-zinc-solubility electrolytes for use in zinc/nickel oxide cells," *J. Electrochem. Soc.*, vol. 140, no. 2, pp. 289–294, 1993.

[75] R. Renuka, S. Ramamurthy, and L. Srinivasan, "Interaction of zincate with additives turbidimetric, IR and Raman spectral analyses," *J. Power Sources*, vol. 89, no. 1, pp. 70–79, 2000.

[76] I. Arise, Y. Fukunaka, and F. McLarnon, "Ionic mass transfer accompanying anodic dissolution of zinc in alkaline solution," *J. Electrochem. Soc.*, vol. 153, no. 1, pp. A69–A74, 2006.

[77] Y.-H. Wen, J. Cheng, L. Zhang, X. Yan, and Y.-S. Yang, "The inhibition of the spongy electrocrystallization of zinc from doped flowing alkaline zincate solutions," *J. Power Sources*, vol. 193, no. 2, pp. 890–894, 2009.

[78] B. Sharifi, M. Mojtahedi, M. Goodarzi, and J. V. Khaki, "Effect of alkaline electrolysis conditions on current efficiency and morphology of zinc powder," *Hydrometallurgy*, vol. 99, no. 1, pp. 72–76, 2009.

[79] M. Simičić, K. Popov, and N. Krstajić, "An experimental study of zinc morphology in alkaline electrolyte at low direct and pulsating overpotentials," *J. Electroanal. Chem.*, vol. 484, no. 1, pp. 18–23, 2000.

[80] S. E. Ziemniak, M. E. Jones, and K. E. S. Combs, "Zinc(II) oxide solubility and phase behavior in aqueous sodium phosphate solutions at elevated temperatures," *J. Solution Chem.*, vol. 21, no. 11, pp. 1153–1176, 1992.

[81] M. R. Anseau, J. P. Leung, S. Nita, and T. W. Swaddle, "Interactions of silicate ions with zinc(II) and aluminum(III) in alkaline aqueous solution," *J. Cheminform.*, vol. 44, no. 22, pp. 8023–8032, 2005.

[82] A. R. Mainar, O. Leonet, M. Bengoechea, I. Boyano, I. Meatza, A. Kvasha, A. Guerfi, and J. A. Blázquez, "Alkaline aqueous electrolytes for secondary zinc–air batteries: An overview," *Int. J. Renew. Energy Res.*, vol. 40, pp. 1032–1049, 2016.

[83] J. Fu, J. Zhang, X. Song, H. Zarrin, X. Tian, J. Qiao, L. Rasen, K. Li, and Z. Chen, "A flexible solid-state electrolyte for wide-scale integration of rechargeable zinc–air batteries," *Energy Environ. Sci.*, vol. 9, pp. 663–670, 2016.

[84] R. Cao, J. S. Lee, M. Liu, and J. Cho, "Recent progress in non-precious catalysts for metal–air batteries," *Adv. Energy Mater.*, vol. 2, no. 7, pp. 816–829, 2012.

[85] M. A. Rahman, X. Wang, and C. Wen, "High energy density metal–air batteries: A review," *J. Electrochem. Soc.*, vol. 160, no. 10, pp. A1759–A1771, 2013.

[86] B. Xia, Y. Yan, X. Wang, and X. W. D. Lou, "Recent progress on graphene-based hybrid electrocatalysts," *Mater. Horiz.*, vol. 1, no. 4, pp. 379–399, 2014.

[87] C. Zhu and S. Dong, "Recent progress in graphene-based nanomaterials as advanced electrocatalysts towards oxygen reduction reaction," *Nanoscale*, vol. 5, no. 5, pp. 1753–1767, 2013.

[88] C. Yuan, H. B. Wu, Y. Xie, and X. W. D. Lou, "Mixed transition-metal oxides: Design, synthesis, and energy-related applications," *Angew. Chem. Int. Ed.*, vol. 53, no. 6, pp. 1488–1504, 2014.

[89] R. Black, B. Adams, and L. Nazar, "Non-aqueous and hybrid Li-O2 batteries," *Adv. Energy Mater.*, vol. 2, no. 7, pp. 801–815, 2012.

[90] J. Christensen, P. Albertus, R. S. Sanchez-Carrera, T. Lohmann, B. Kozinsky, R. Liedtke, J. Ahmed, and A. Kojic, "A critical review of Li/air batteries," *J. Electrochem. Soc.*, vol. 159, no. 2, pp. R1–R30, 2011.

[91] D. Higgins, P. Zamani, A. Yu, and Z. Chen, "The application of graphene and its composites in oxygen reduction electrocatalysis: A perspective and review of recent progress," *Energy Environ. Sci.*, vol. 9, pp. 357–390, 2016.

[92] Y. Shao, S. Park, J. Xiao, J.-G. Zhang, Y. Wang, and J. Liu, "Electrocatalysts for nonaqueous lithium–air batteries: status, challenges, and perspective," *ACS Catal.*, vol. 2, no. 5, pp. 844–857, 2012.

[93] V. Neburchilov, H. Wang, J. J. Martin, and W. Qu, "A review on air cathodes for zinc–air fuel cells," *J. Power Sources*, vol. 195, no. 5, pp. 1271–1291, 2010.

[94] H. Wang and H. Dai, "Strongly coupled inorganic–nano-carbon hybrid materials for energy storage," *Chem. Soc. Rev.*, vol. 42, no. 7, pp. 3088–3113, 2013.

[95] M. Zhou, H.-L. Wang, and S. Guo, "Towards high-efficiency nanoelectrocatalysts for oxygen reduction through engineering advanced carbon nanomaterials," *Chem. Soc. Rev.*, 2016.

[96] Q. Li, R. Cao, J. Cho, and G. Wu, "Nanostructured carbon-based cathode catalysts for nonaqueous lithium–oxygen batteries," *Phys. Chem. Chem. Phys.*, vol. 16, no. 27, pp. 13568–13582, 2014.

[97] D. Capsoni, M. Bini, S. Ferrari, E. Quartarone, and P. Mustarelli, "Recent advances in the development of Li–air batteries," *J. Power Sources*, vol. 220, pp. 253–263, 2012.

[98] F. Li, T. Zhang, and H. Zhou, "Challenges of non-aqueous Li–O 2 batteries: Electrolytes, catalysts, and anodes," *Energy Environ. Sci.*, vol. 6, no. 4, pp. 1125–1141, 2013.

[99] Z. Wen, C. Shen, and Y. Lu, "Air electrode for the lithium–air batteries: Materials and structure designs," *Chempluschem.*, vol. 80, no. 2, pp. 270–287, 2015.

[100] D. Egan, C. P. De León, R. Wood, R. Jones, K. Stokes, and F. Walsh, "Developments in electrode materials and electrolytes for aluminium–air batteries," *J. Power Sources*, vol. 236, pp. 293–310, 2013.

[101] J. Martin, V. Neburchilov, H. Wang, and W. Qu, "Air cathodes for metal–air batteries and fuel cells," in *Proc. IEEE Electrical Power & Energy Conf.*, 2009, pp. 1–6.

[102] J. S. Spendelow and A. Wieckowski, "Electrocatalysis of oxygen reduction and small alcohol oxidation in alkaline media," *Phys. Chem. Chem. Phys.*, vol. 9, no. 21, pp. 2654–2675, 2007.

[103] P. Christensen, A. Hamnett, and D. Linares-Moya, "Oxygen reduction and fuel oxidation in alkaline solution," *Phys. Chem. Chem. Phys.*, vol. 13, no. 12, pp. 5206–5214, 2011.

[104] D. Wilkinson, J. St-Pierre, W. Vielstich, H. Gasteiger, and A. Lamm, "Handbook of fuel cells–fundamentals, technology and applications," in *Fuel cell Technology and Applications.* Hoboken, NJ: Wiley, 2009.

[105] M. Bajdich, M. N. García-Mota, A. Vojvodic, J. K. Nørskov, and A. T. Bell, "Theoretical investigation of the activity of cobalt oxides for the electrochemical oxidation of water," *J. Am. Chem. Soc.*, vol. 135, no. 36, pp. 13521–13530, 2013.

[106] A. Valdes, J. Brillet, M. Grätzel, H. Gudmundsdottir, H. A. Hansen, H. Jónsson, P. Klüpfel, G.-J. Kroes, F. Le Formal, and I. C. Man, "Solar hydrogen production with semiconductor metal oxides: New directions in experiment and theory," *Phys. Chem. Chem. Phys.*, vol. 14, no. 1, pp. 49–70, 2012.

[107] J. K. Nørskov, T. Bligaard, A. Logadottir, S. Bahn, L. B. Hansen, M. Bollinger, H. Bengaard, B. Hammer, Z. Sljivancanin, and M. Mavrikakis, "Universality in heterogeneous catalysis," *J. Catal.*, vol. 209, no. 2, pp. 275–278, 2002.

[108] S. Trasatti, "Electrocatalysis by oxides—attempt at a unifying approach," *J. Electroanal. Chem. Interfacial Electrochem.*, vol. 111, no. 1, pp. 125–131, 1980.

[109] J. O. M. Bockris and T. Otagawa, "The electrocatalysis of oxygen evolution on perovskites," *J. Electrochem. Soc.*, vol. 131, no. 2, pp. 290–302, 1984.

[110] J. Rossmeisl, Z.-W. Qu, H. Zhu, G.-J. Kroes, and J. K. Nørskov, "Electrolysis of water on oxide surfaces," *J. Electroanal. Chem.*, vol. 607, no. 1, pp. 83–89, 2007.

[111] I. C. Man, H. Y. Su, F. Calle-Vallejo, H. A. Hansen, J. I. Martínez, N. G. Inoglu, J. Kitchin, T. F. Jaramillo, J. K. Nørskov, and J. Rossmeisl,

"Universality in oxygen evolution electrocatalysis on oxide surfaces," *ChemCatChem.*, vol. 3, no. 7, pp. 1159–1165, 2011.
[112] Z. Chen, D. Higgins, A. Yu, L. Zhang, and J. Zhang, "A review on non-precious metal electrocatalysts for PEM fuel cells," *Energy Environ. Sci.*, vol. 4, no. 9, pp. 3167–3192, 2011.
[113] H. Cheng and K. Scott, "Carbon-supported manganese oxide nanocatalysts for rechargeable lithium–air batteries," *J. Power Sources*, vol. 195, no. 5, pp. 1370–1374, 2010.
[114] D. Zhang, Z. Fu, Z. Wei, T. Huang, and A. Yu, "Polarization of oxygen electrode in rechargeable lithium oxygen batteries," *J. Electrochem. Soc.*, vol. 157, no. 3, pp. A362–A365, 2010.
[115] X. Han, F. Cheng, C. Chen, Y. Hu, and J. Chen, "Uniform MnO2 nanostructures supported on hierarchically porous carbon as efficient electrocatalysts for rechargeable Li-O2 batteries," *Nano Res.*, vol. 8, no. 1, pp. 156–164, 2015.
[116] P. Żółtowski, D. Dražić, and L. Vorkapić, "Carbon-air electrode with regenerative short time overload capacity: Part 1. Effect of manganese dioxide," *J. Appl. Electrochem.*, vol. 3, no. 4, pp. 271–283, 1973.
[117] L. Mao, T. Sotomura, K. Nakatsu, N. Koshiba, D. Zhang, and T. Ohsaka, "Electrochemical characterization of catalytic activities of manganese oxides to oxygen reduction in alkaline aqueous solution," *J. Electrochem. Soc.*, vol. 149, no. 4, pp. A504–A507, 2002.
[118] T. Ohsaka, L. Mao, K. Arihara, and T. Sotomura, "Bifunctional catalytic activity of manganese oxide toward O2 reduction: Novel insight into the mechanism of alkaline air electrode," *Electrochem. Commun.*, vol. 6, no. 3, pp. 273–277, 2004.
[119] A. K. Thapa and T. Ishihara, "Mesoporous $\alpha$-MnO 2/Pd catalyst air electrode for rechargeable lithium–air battery," *J. Power Sources*, vol. 196, no. 16, pp. 7016–7020, 2011.
[120] F. Cheng, Y. Su, J. Liang, Z. Tao, and J. Chen, "MnO2-based nanostructures as catalysts for electrochemical oxygen reduction in alkaline media," *Chem. Mater.*, vol. 22, no. 3, pp. 898–905, 2010.
[121] A. Débart, A. J. Paterson, J. Bao, and P. G. Bruce, "$\alpha$-MnO2 nanowires: A catalyst for the O2 electrode in rechargeable lithium batteries," *Angew. Chem. Int. Ed.*, vol. 120, no. 24, pp. 4597–4600, 2008.
[122] J. Brenet, "Electrochemical behaviour of metallic oxides," *J. Power Sources*, vol. 4, no. 3, pp. 183–190, 1979.
[123] L. Mao, D. Zhang, T. Sotomura, K. Nakatsu, N. Koshiba, and T. Ohsaka, "Mechanistic study of the reduction of oxygen in air electrode with manganese oxides as electrocatalysts," *Electrochim. Acta*, vol. 48, no. 8, pp. 1015–1021, 2003.
[124] Q. Tang, L. Jiang, J. Liu, S. Wang, and G. Sun, "Effect of surface manganese valence of manganese oxides on the activity of the oxygen reduction reaction in alkaline media," *ACS Catal.*, vol. 4, no. 2, pp. 457–463, 2014.
[125] J. Suntivich, H. A. Gasteiger, N. Yabuuchi, H. Nakanishi, J. B. Goodenough, and Y. Shao-Horn, "Design principles for oxygen-reduction activity on perovskite oxide catalysts for fuel cells and metal–air batteries," *Nature Chem.*, vol. 3, no. 7, pp. 546–550, 2011.
[126] M. Sugawara, M. Ohno, and K. Matsuki, "Oxygen reduction catalysis of Mn–Co spinel oxides on a graphite electrode in alkaline solution," *J. Mater. Chem.*, vol. 7, no. 5, pp. 833–836, 1997.
[127] Y. Liang, H. Wang, J. Zhou, Y. Li, J. Wang, T. Regier, and H. Dai, "Covalent hybrid of spinel manganese–cobalt oxide and graphene as advanced oxygen reduction electrocatalysts," *J. Am. Chem. Soc.*, vol. 134, no. 7, pp. 3517–3523, 2012.
[128] H. Liu, X. Zhu, M. Li, Q. Tang, G. Sun, and W. Yang, "Single crystal (Mn, Co) 3 O 4 octahedra for highly efficient oxygen reduction reactions," *Electrochim. Acta*, vol. 144, pp. 31–41, 2014.
[129] E. Rios, J.-L. Gautier, G. Poillerat, and P. Chartier, "Mixed valency spinel oxides of transition metals and electrocatalysis: Case of the Mn x Co 3– x O 4 system," *Electrochim. Acta*, vol. 44, no. 8, pp. 1491–1497, 1998.
[130] E. Lee, J.-H. Jang, and Y.-U. Kwon, "Composition effects of spinel Mn x Co 3– x O 4 nanoparticles on their electrocatalytic properties in oxygen reduction reaction in alkaline media," *J. Power Sources*, vol. 273, pp. 735–741, 2015.
[131] M. Hamdani, R. Singh, and P. Chartier, "Co3O4 and Co-based spinel oxides bifunctional oxygen electrodes," *Int. J. Electrochem. Sci.*, vol. 5, no. 4, 556, 2010.
[132] L. Hu, L. Wu, M. Liao, X. Hu, and X. Fang, "Electrical transport properties of large, individual NiCo2O4 nanoplates," *Adv. Funct. Mater.*, vol. 22, no. 5, pp. 998–1004, 2012.
[133] C. Li, X. Han, F. Cheng, Y. Hu, C. Chen, and J. Chen, "Phase and composition controllable synthesis of cobalt manganese spinel nanoparticles towards efficient oxygen electrocatalysis," *Nature Commun.*, vol. 6, pp. 7345–7352, 2015.
[134] T. Maiyalagan, K. A. Jarvis, S. Therese, P. J. Ferreira, and A. Manthiram, "Spinel-type lithium cobalt oxide as a bifunctional electrocatalyst for the oxygen evolution and oxygen reduction reactions," *Nature Commun.*, vol. 5, pp. 3949–3956, 2014.
[135] J. Li, M. Zou, W. Wen, Y. Zhao, Y. Lin, L. Chen, H. Lai, L. Guan, and Z. Huang, "Spinel MFe 2 O 4 (M= Co, Ni) nanoparticles coated on multi-walled carbon nanotubes as electrocatalysts for Li–O 2 batteries," *J. Mater. Chem. A*, vol. 2, no. 26, pp. 10257–10262, 2014.
[136] Z. Pu, Q. Liu, C. Tang, A. M. Asiri, A. H. Qusti, A. O. Al-Youbi, and X. Sun, "Spinel ZnCo 2 O 4/N-doped carbon nanotube composite: A high active oxygen reduction reaction electrocatalyst," *J. Power Sources*, vol. 257, pp. 170–173, 2014.
[137] G. Wu, J. Wang, W. Ding, Y. Nie, L. Li, X. Qi, S. Chen, and Z. Wei, "A strategy to promote the electrocatalytic activity of spinels for oxygen reduction by structure reversal," *Angew. Chem. Int. Ed.*, vol. 55, pp. 1340–1344, 2016.
[138] T. Maiyalagan, K. R. Chemelewski, and A. Manthiram, "Role of the morphology and surface planes on the catalytic activity of spinel LiMn1. 5Ni0. 5O4 for oxygen evolution reaction," *ACS Catal.*, vol. 4, no. 2, pp. 421–425, 2014.
[139] X. Ge, Y. Liu, F. T. Goh, T. A. Hor, Y. Zong, P. Xiao, Z. Zhang, S. H. Lim, B. Li, and X. Wang, "Dual-phase spinel MnCo2O4 and spinel MnCo2O4/nanocarbon hybrids for electrocatalytic oxygen reduction and evolution," *ACS Appl. Mater. Interfaces*, vol. 6, no. 15, pp. 12684–12691, 2014.
[140] A. Zhao, J. Masa, W. Xia, A. Maljusch, M.-G. Willinger, G. Clavel, K. Xie, R. Schlögl, W. Schuhmann, and M. Muhler, "Spinel Mn–Co oxide in N-doped carbon nanotubes as a bifunctional electrocatalyst synthesized by oxidative cutting," *J. Am. Chem. Soc.*, vol. 136, no. 21, pp. 7551–7554, 2014.
[141] C. Li, X. Han, F. Cheng, Y. Hu, C. Chen, and J. Chen, "Phase and composition controllable synthesis of cobalt manganese spinel nanoparticles towards efficient oxygen electrocatalysis," *Nature Commun.*, vol. 6, p. 7345, 2015.
[142] F. Cheng, J. Shen, B. Peng, Y. Pan, Z. Tao, and J. Chen, "Rapid room-temperature synthesis of nanocrystalline spinels as oxygen reduction and evolution electrocatalysts," *Nature Chem.*, vol. 3, no. 1, pp. 79–84, 2011.
[143] T. Wolfram and S. Ellialtioglu, *Electronic and Optical Properties of d-Band Perovskites*. Cambridge, U.K.: Cambridge Univ. Press, 2006.
[144] W. G. Hardin, J. T. Mefford, D. A. Slanac, B. B. Patel, X. Wang, S. Dai, X. Zhao, R. S. Ruoff, K. P. Johnston, and K. J. Stevenson, "Tuning the electrocatalytic activity of perovskites through active site variation and support interactions," *Chem. Mater.*, vol. 26, no. 11, pp. 3368–3376, 2014.
[145] Z. Du, P. Yang, L. Wang, Y. Lu, J. Goodenough, J. Zhang, and D. Zhang, "Electrocatalytic performances of LaNi 1– x Mg x O 3 perovskite oxides as bi-functional catalysts for lithium air batteries," *J. Power Sources*, vol. 265, pp. 91–96, 2014.
[146] H. Zhang, Y. Shimizu, Y. Teraoka, N. Miura, and N. Yamazoe, "Oxygen sorption and catalytic properties of La 1– x Sr x Co 1– y Fe y O 3 perovskite-type oxides," *J. Catalysis*, vol. 121, no. 2, pp. 432–440, 1990.
[147] S. Zou, M. S. Burke, M. G. Kast, J. Fan, N. Danilovic, and S. W. Boettcher, "Fe (oxy) hydroxide oxygen evolution reaction electrocatalysis: intrinsic activity and the roles of electrical conductivity, substrate, and dissolution," *Chem. Mater.*, vol. 27, no. 23, pp. 8011–8020, 2015.
[148] K. Mette, A. Bergmann, J. P. Tessonnier, M. Hävecker, L. Yao, T. Ressler, R. Schlögl, P. Strasser, and M. Behrens, "Nanostructured manganese oxide supported on carbon nanotubes for electrocatalytic water splitting," *ChemCatChem.*, vol. 4, no. 6, pp. 851–862, 2012.
[149] A. Ramírez, P. Bogdanoff, D. Friedrich, and S. Fiechter, "Synthesis of Ca 2 Mn 3 O 8 films and their electrochemical studies for the oxygen evolution reaction (OER) of water," *Nano Energy*, vol. 1, no. 2, pp. 282–289, 2012.
[150] D. M. Robinson, Y. B. Go, M. Mui, G. Gardner, Z. Zhang, D. Mastrogiovanni, E. Garfunkel, J. Li, M. Greenblatt, and G. C. Dismukes, "Photochemical water oxidation by crystalline polymorphs of manganese oxides: Structural requirements for catalysis," *J. Am. Chem. Soc.*, vol. 135, no. 9, pp. 3494–3501, 2013.
[151] Y. Gorlin, B. Lassalle-Kaiser, J. D. Benck, S. Gul, S. M. Webb, V. K. Yachandra, J. Yano, and T. F. Jaramillo, "In situ X-ray absorption spectroscopy investigation of a bifunctional manganese oxide catalyst with high activity for electrochemical water oxidation and oxygen reduction," *J. Am. Chem. Soc.*, vol. 135, no. 23, pp. 8525–8534, 2013.
[152] V. Rashkova, S. Kitova, I. Konstantinov, and T. Vitanov, "Vacuum evaporated thin films of mixed cobalt and nickel oxides as electrocatalyst for oxygen evolution and reduction," *Electrochim. Acta*, vol. 47, no. 10, pp. 1555–1560, 2002.
[153] L. Jörissen, "Bifunctional oxygen/air electrodes," *J. Power Sources*, vol. 155, no. 1, pp. 23–32, 2006.
[154] Y. Liang, H. Wang, P. Diao, W. Chang, G. Hong, Y. Li, M. Gong, L. Xie, J. Zhou, and J. Wang, "Oxygen reduction electrocatalyst based on strongly coupled cobalt oxide nanocrystals and carbon nanotubes," *J. Am. Chem. Soc.*, vol. 134, no. 38, pp. 15,849–15,857, 2012.
[155] Y. J. Sa, K. Kwon, J. Y. Cheon, F. Kleitz, and S. H. Joo, "Ordered mesoporous Co 3 O 4 spinels as stable, bifunctional, noble metal-free oxygen electrocatalysts," *J. Mater. Chem. A*, vol. 1, no. 34, pp. 9992–10,001, 2013.
[156] G. Wu, N. Li, D.-R. Zhou, K. Mitsuo, and B.-Q. Xu, "Anodically electrodeposited Co+ Ni mixed oxide electrode: preparation and electrocatalytic activity for oxygen evolution in alkaline media," *J. Solid State Chem.*, vol. 177, no. 10, pp. 3682–3692, 2004.
[157] H. Zhu, S. Zhang, Y.-X. Huang, L. Wu, and S. Sun, "Monodisperse M x Fe3–x O4 (M= Fe, Cu, Co, Mn) nanoparticles and their electrocatalysis for oxygen reduction reaction," *Nano Lett.*, vol. 13, no. 6, pp. 2947–2951, 2013.
[158] M. De Koninck and B. Marsan, "Mn x Cu 1– x Co 2 O 4 used as bifunctional electrocatalyst in alkaline medium," *Electrochim. Acta*, vol. 53, no. 23, pp. 7012–7021, 2008.
[159] J. Landon, E. Demeter, N. İnoğlu, C. Keturakis, I. E. Wachs, R. Vasić, A. I. Frenkel, and J.

R. Kitchin, "Spectroscopic characterization of mixed Fe–Ni oxide electrocatalysts for the oxygen evolution reaction in alkaline electrolytes," *ACS Catal.*, vol. 2, no. 8, pp. 1793–1801, 2012.

[160] J. Ponce, J.-L. Rehspringer, G. Poillerat, and J. Gautier, "Electrochemical study of nickel–aluminium–manganese spinel Ni x Al 1– x Mn 2 O 4. Electrocatalytical properties for the oxygen evolution reaction and oxygen reduction reaction in alkaline media," *Electrochim. Acta*, vol. 46, no. 22, pp. 3373–3380, 2001.

[161] D. U. Lee, B. J. Kim, and Z. Chen, "One-pot synthesis of a mesoporous NiCo 2 O 4 nanoplatelet and graphene hybrid and its oxygen reduction and evolution activities as an efficient bi-functional electrocatalyst," *J. Mater. Chem. A*, vol. 1, no. 15, pp. 4754–4762, 2013.

[162] N. Li, X. Yan, W. Zhang, and B. Lin, "Electrocatalytic activity of spinel-type oxides LiMn 2– X Co X O 4 with large specific surface areas for metal–air battery," *J. Power Sources*, vol. 74, no. 2, pp. 255–258, 1998.

[163] W. Yang, J. Salim, S. Li, C. Sun, L. Chen, J. B. Goodenough, and Y. Kim, "Perovskite Sr 0.95 Ce 0.05 CoO 3– $\delta$ loaded with copper nanoparticles as a bifunctional catalyst for lithium-air batteries," *J. Mater. Chem.*, vol. 22, no. 36, pp. 18,902–18,907, 2012.

[164] Y. Lee, J. Suntivich, K. J. May, E. E. Perry, and Y. Shao-Horn, "Synthesis and activities of rutile IrO2 and RuO2 nanoparticles for oxygen evolution in acid and alkaline solutions," *J. Phys. Chem. Lett.*, vol. 3, no. 3, pp. 399–404, 2012.

[165] B. Sun, P. Munroe, and G. Wang, "Ruthenium nanocrystals as cathode catalysts for lithium–oxygen batteries with a superior performance," *Scientific Rep.*, vol. 3, 2013.

[166] C. V. Rao and B. Viswanathan, "Ru x Se y/C electrodes for oxygen reduction a reverse microemulsion method of fabrication of electrode material," *J. Phys. Chem. C*, vol. 111, no. 44, pp. 16538–16543, 2007.

[167] R. Subbaraman, D. Tripkovic, K.-C. Chang, D. Strmcnik, A. P. Paulikas, P. Hirunsit, M. Chan, J. Greeley, V. Stamenkovic, and N. M. Markovic, "Trends in activity for the water electrolyser reactions on 3d M (Ni, Co, Fe, Mn) hydr (oxy) oxide catalysts," *Nature Mater.*, vol. 11, no. 6, pp. 550–557, 2012.

[168] D. K. Bediako, B. Lassalle-Kaiser, Y. Surendranath, J. Yano, V. K. Yachandra, and D. G. Nocera, "Structure–activity correlations in a nickel–borate oxygen evolution catalyst," *J. Am. Chem. Soc.*, vol. 134, no. 15, pp. 6801–6809, 2012.

[169] J. O. Bockris and T. Otagawa, "Mechanism of oxygen evolution on perovskites," *J. Phys. Chem.*, vol. 87, no. 15, pp. 2960–2971, 1983.

[170] L. Trotochaud, J. K. Ranney, K. N. Williams, and S. W. Boettcher, "Solution-cast metal oxide thin film electrocatalysts for oxygen evolution," *J. Am. Chem. Soc.*, vol. 134, no. 41, pp. 17,253–17,261, 2012.

[171] D. M. Robinson, Y. B. Go, M. Greenblatt, and G. C. Dismukes, "Water oxidation by $\lambda$-MnO2: catalysis by the cubical Mn4O4 subcluster obtained by delithiation of spinel LiMn2O4," *J. Am. Chem. Soc.*, vol. 132, no. 33, pp. 11,467–11,469, 2010.

[172] F. Jiao and H. Frei, "Nanostructured cobalt and manganese oxide clusters as efficient water oxidation catalysts," *Energy Environ. Sci.*, vol. 3, no. 8, pp. 1018–1027, 2010.

[173] G. P. Gardner, Y. B. Go, D. M. Robinson, P. F. Smith, J. Hadermann, A. Abakumov, M. Greenblatt, and G. C. Dismukes, "Structural requirements in lithium cobalt oxides for the catalytic oxidation of water," *Angew. Chem. Int. Ed.*, vol. 51, no. 7, pp. 1616–1619, 2012.

[174] J. Suntivich, K. J. May, H. A. Gasteiger, J. B. Goodenough, and Y. Shao-Horn, "A perovskite oxide optimized for oxygen evolution catalysis from molecular orbital principles," *Science*, vol. 334, no. 6061, pp. 1383–1385, 2011.

[175] C. Davidson, G. Kissel, and S. Srinivasan, "Electrode kinetics of the oxygen evolution reaction at NiCo 2 O 4 from 30% KOH: Dependence on temperature," *J. Electroanal. Chem. Interfacial Electrochem.*, vol. 132, pp. 129–135, 1982.

[176] H. Tanaka and M. Misono, "Advances in designing perovskite catalysts," *Curr. Opin. Solid State Mater. Sci.*, vol. 5, no. 5, pp. 381–387, 2001.

[177] Y. Gorlin and T. F. Jaramillo, "A bifunctional nonprecious metal catalyst for oxygen reduction and water oxidation," *J. Am. Chem. Soc.*, vol. 132, no. 39, pp. 13,612–13,614, 2010.

[178] K. R. Yoon, G. Y. Lee, J.-W. Jung, N.-H. Kim, S. O. Kim, and I.-D. Kim, "One-dimensional RuO2/Mn2O3 hollow architectures as efficient bifunctional catalysts for lithium–oxygen batteries," *Nano Lett.*, vol. 16, no. 3, pp. 2076–2083, 2016.

[179] H. Horowitz, J. Longo, and H. Horowitz, "Oxygen electrocatalysis on some oxide pyrochlores," *J. Electrochem. Soc.*, vol. 130, no. 9, pp. 1851–1859, 1983.

[180] J. B. Goodenough, R. Manoharan, and M. Paranthaman, "Surface protonation and electrochemical activity of oxides in aqueous solution," *J. Am. Chem. Soc.*, vol. 112, no. 6, pp. 2076–2082, 1990.

[181] S. H. Oh, R. Black, E. Pomerantseva, J.-H. Lee, and L. F. Nazar, "Synthesis of a metallic mesoporous pyrochlore as a catalyst for lithium–O2 batteries," *Nature Chem.*, vol. 4, no. 12, pp. 1004–1010, 2012.

[182] J.-M. Zen, R. Manoharan, and J. Goodenough, "Oxygen reduction on Ru-oxide pyrochlores bonded to a proton-exchange membrane," *J. Appl. Electrochem.*, vol. 22, no. 2, pp. 140–150, 1992.

[183] H. Horowitz, J. Longo, and J. Lewandowski, "New oxide pyrochlores: A 2 [B 2– x A x] O 7– y (A= Pb, Bi; B= Ru, Ir)," *Mater. Res. Bull.*, vol. 16, no. 5, pp. 489–496, 1981.

[184] T. Takeda, R. Kanno, Y. Kawamoto, Y. Takeda, and O. Yamamoto, "New cathode materials for solid oxide fuel cells ruthenium pyrochlores and perovskites," *J. Electrochem. Soc.*, vol. 147, no. 5, pp. 1730–1733, 2000.

[185] G. Liu, X. Li, J.-W. Lee, and B. N. Popov, "A review of the development of nitrogen-modified carbon-based catalysts for oxygen reduction at USC," *Catal. Sci. Tech.*, vol. 1, no. 2, pp. 207–217, 2011.

[186] H. Tributsch, "Multi-electron transfer catalysis for energy conversion based on abundant transition metals," *Electrochim. Acta*, vol. 52, no. 6, pp. 2302–2316, 2007.

[187] F. Jaouen, E. Proietti, M. Lefèvre, R. Chenitz, J.-P. Dodelet, G. Wu, H. T. Chung, C. M. Johnston, and P. Zelenay, "Recent advances in non-precious metal catalysis for oxygen-reduction reaction in polymer electrolyte fuel cells," *Energy Environ. Sci.*, vol. 4, no. 1, pp. 114–130, 2011.

[188] W. Xia, A. Mahmood, Z. Liang, R. Zou, and S. Guo, "Earth-abundant nanomaterials for oxygen reduction," *Angew. Chem. Int. Ed.*, vol. 54, pp. 2–29, 2015.

[189] A. Tanaka, C. Fierro, D. Scherson, and E. Yaeger, "Electrocatalytic aspects of iron phthalocyanine and its mu–oxo derivatives dispersed on high surface area carbon," *J. Phys. Chem*, vol. 91, no. 14, pp. 3799–3807, 1987.

[190] C. W. Bezerra, L. Zhang, K. Lee, H. Liu, A. L. Marques, E. P. Marques, H. Wang, and J. Zhang, "A review of Fe–N/C and Co–N/C catalysts for the oxygen reduction reaction," *Electrochim. Acta*, vol. 53, no. 15, pp. 4937–4951, 2008.

[191] A. A. Gewirth and M. S. Thorum, "Electroreduction of dioxygen for fuel-cell applications: materials and challenges," *Inorg. Chem.*, vol. 49, no. 8, pp. 3557–3566, 2010.

[192] J. P. Collman, P. Denisevich, Y. Konai, M. Marrocco, C. Koval, and F. C. Anson, "Electrode catalysis of the four-electron reduction of oxygen to water by dicobalt face-to-face porphyrins," *J. Am. Chem. Soc.*, vol. 102, no. 19, pp. 6027–6036, 1980.

[193] M. Lefevre, J. Dodelet, and P. Bertrand, "O2 reduction in PEM fuel cells: activity and active site structural information for catalysts obtained by the pyrolysis at high temperature of Fe precursors," *J. Phys. Chem. B*, vol. 104, no. 47, pp. 11238–11247, 2000.

[194] V. Bagotzky, M. Tarasevich, K. Radyushkina, O. Levina, and S. Andrusyova, "Electrocatalysis of the oxygen reduction process on metal chelates in acid electrolyte," *J. Power Sources*, vol. 2, no. 3, pp. 233–240, 1978.

[195] C. W. Bezerra, L. Zhang, H. Liu, K. Lee, A. L. Marques, E. P. Marques, H. Wang, and J. Zhang, "A review of heat-treatment effects on activity and stability of PEM fuel cell catalysts for oxygen reduction reaction," *J. Power Sources*, vol. 173, no. 2, pp. 891–908, 2007.

[196] H. Jahnke, M. Schönborn, and G. Zimmermann, "Organic dyestuffs as catalysts for fuel cells," in *Physical and chemical applications of dyestuffs*, F. P. Schäfer, H. Gerischer, F. Willig, H. Meier, H. Jahnke, M. Schönborn, and G. Zimmermann, Eds. New York: Springer-Verlag, 1976, pp. 133–181.

[197] J. Masa, W. Xia, I. Sinev, A. Zhao, Z. Sun, S. Grützke, P. Weide, M. Muhler, and W. Schuhmann, "MnxOy/NC and CoxOy/NC nanoparticles embedded in a nitrogen-doped carbon matrix for high-performance bifunctional oxygen electrodes," *Angew. Chem. Int. Ed.*, vol. 53, no. 32, pp. 8508–8512, 2014.

[198] P. Bogdanoff, I. Herrmann, M. Hilgendorff, I. Dorbandt, S. Fiechter, and H. Tributsch, "Probing structural effects of pyrolysed CoTMPP-based electrocatalysts for oxygen reduction via new preparation strategies," *J. New Mater. Electrochem. Syst.*, vol. 7, no. 2, pp. 85–92, 2004.

[199] R. Jasinski, "A new fuel cell cathode catalyst," 1964.

[200] J. P. Collman, P. S. Wagenknecht, and J. E. Hutchison, "Molecular catalysts for multielectron redox reactions of small molecules: The "Cofacial metallodiporphyrin" approach," *Angew. Chem. Int. Ed. Engl.*, vol. 33, no. 15–16, pp. 1537–1554, 1994.

[201] C. Chang, H. Liu, and I. Abdalmuhdi, "Electroreduction of oxygen by pillared cobalt (II) cofacial diporphyrin catalysts," *J. Am. Chem. Soc.*, vol. 106, no. 9, pp. 2725–2726, 1984.

[202] C. J. Chang, Z.-H. Loh, C. Shi, F. C. Anson, and D. G. Nocera, "Targeted proton delivery in the catalyzed reduction of oxygen to water by bimetallic pacman porphyrins," *J. Am. Chem. Soc.*, vol. 126, no. 32, pp. 10,013–10,020, 2004.

[203] R. Liu, C. von Malotki, L. Arnold, N. Koshino, H. Higashimura, M. Baumgarten, and K. Müllen, "Triangular trinuclear metal-N4 complexes with high electrocatalytic activity for oxygen reduction," *J. Am. Chem. Soc.*, vol. 133, no. 27, pp. 10372–10375, 2011.

[204] T. Sun, Q. Wu, R. Che, Y. Bu, Y. Jiang, Y. Li, L. Yang, X. Wang, and Z. Hu, "Alloyed Co–Mo nitride as high-performance electrocatalyst for oxygen reduction in acidic medium," *ACS Catal.*, vol. 5, no. 3, pp. 1857–1862, 2015.

[205] T. Ando, S. Izhar, H. Tominaga, and M. Nagai, "Ammonia-treated carbon-supported cobalt tungsten as fuel cell cathode catalyst," *Electrochim. Acta*, vol. 55, no. 8, pp. 2614–2621, 2010.

[206] X. Tian, J. Luo, H. Nan, Z. Fu, J. Zeng, and S. Liao, "Binary transition metal nitrides with enhanced activity and durability for the oxygen reduction reaction," *J. Mater. Chem. A*, vol. 3, no. 32, pp. 16,801–16,809, 2015.

[207] J. Xie and Y. Xie, "Transition metal nitrides for electrocatalytic energy conversion: Opportunities

and challenges," *Eur. J. Inorg. Chem.*, vol. 22, pp. 3588–3598, 2015.
[208] E. B. Easton, R. Yang, A. Bonakdarpour, and J. Dahn, "Thermal evolution of the structure and activity of magnetron-sputtered TM–C–N (TM = Fe, Co) oxygen reduction catalysts," *Electrochem. Solid-State Lett.*, vol. 10, no. 1, pp. B6–B10, 2007.
[209] E. B. Easton, A. Bonakdarpour, R. Yang, D. A. Stevens, and J. Dahn, "Magnetron sputtered Fe–C–N, Fe–C, and C–N based oxygen reduction electrocatalysts," *J. Electrochem. Soc.*, vol. 155, no. 6, pp. B547–B557, 2008.
[210] R. Yang, K. Stevens, and J. Dahn, "Investigation of activity of sputtered transition-metal (TM)–C–N (TM = V, Cr, Mn, Co, Ni) catalysts for oxygen reduction reaction," *J. Electrochem. Soc.*, vol. 155, no. 1, pp. B79–B91, 2008.
[211] E. Frackowiak and F. Beguin, "Carbon materials for the electrochemical storage of energy in capacitors," *Carbon*, vol. 39, no. 6, pp. 937–950, 2001.
[212] R. Bashyam and P. Zelenay, "A class of non-precious metal composite catalysts for fuel cells," *Nature*, vol. 443, no. 7107, pp. 63–66, 2006.
[213] M. Prabu, K. Ketpang, and S. Shanmugam, "Hierarchical nanostructured NiCo 2 O 4 as an efficient bifunctional non-precious metal catalyst for rechargeable zinc–air batteries," *Nanoscale*, vol. 6, no. 6, pp. 3173–3181, 2014.
[214] G. Wu, N. H. Mack, W. Gao, S. Ma, R. Zhong, J. Han, J. K. Baldwin, and P. Zelenay, "Nitrogen-doped graphene-rich catalysts derived from heteroatom polymers for oxygen reduction in nonaqueous lithium–O2 battery cathodes," *ACS Nano*, vol. 6, no. 11, pp. 9764–9776, 2012.
[215] Z. Chen, A. Yu, D. Higgins, H. Li, H. Wang, and Z. Chen, "Highly active and durable core–corona structured bifunctional catalyst for rechargeable metal–air battery application," *Nano Lett.*, vol. 12, no. 4, pp. 1946–1952, 2012.
[216] Y. Li, W. Zhou, H. Wang, L. Xie, Y. Liang, F. Wei, J.-C. Idrobo, S. J. Pennycook, and H. Dai, "An oxygen reduction electrocatalyst based on carbon nanotube-graphene complexes," *Nature Nanotechnol.*, vol. 7, no. 6, pp. 394–400, 2012.
[217] H. Wang, Y. Yang, Y. Liang, G. Zheng, Y. Li, Y. Cui, and H. Dai, "Rechargeable Li–O 2 batteries with a covalently coupled MnCo 2 O 4–graphene hybrid as an oxygen cathode catalyst," *Energy Environ. Sci.*, vol. 5, no. 7, pp. 7931–7935, 2012.
[218] Y. Liang, Y. Li, H. Wang, J. Zhou, J. Wang, T. Regier, and H. Dai, "Co3O4 nanocrystals on graphene as a synergistic catalyst for oxygen reduction reaction," *Nature Mater.*, vol. 10, no. 10, pp. 780–786, 2011.
[219] O. M. Yaghi, M. O'Keeffe, N. W. Ockwig, H. K. Chae, M. Eddaoudi, and J. Kim, "Reticular synthesis and the design of new materials," *Nature*, vol. 423, no. 6941, pp. 705–714, 2003.
[220] M. O'Keeffe and O. M. Yaghi, "Deconstructing the crystal structures of metal–organic frameworks and related materials into their underlying nets," *Chem. Rev.*, vol. 112, no. 2, pp. 675–702, 2011.
[221] J. J. Perry IV, J. A. Perman, and M. J. Zaworotko, "Design and synthesis of metal–organic frameworks using metal–organic polyhedra as supermolecular building blocks," *Chem. Soc. Rev.*, vol. 38, no. 5, pp. 1400–1417, 2009.
[222] C. Lu, T. Ben, S. Xu, and S. Qiu, "Electrochemical synthesis of a microporous conductive polymer based on a metal–organic framework thin film," *Angew. Chem. Int. Ed.*, vol. 126, no. 25, pp. 6572–6576, 2014.
[223] Q. L. Zhu, W. Xia, T. Akita, R. Zou, and Q. Xu, "Metal-organic framework-derived honeycomb-like open porous nanostructures as precious-metal-free catalysts for highly efficient oxygen electroreduction," *Adv. Mater.*, vol. 28, pp. 6391–6398, 2016.
[224] A. Aijaz, N. Fujiwara, and Q. Xu, "From metal–organic framework to nitrogen-decorated nanoporous carbons: High CO2 uptake and efficient catalytic oxygen reduction," *J. Am. Chem. Soc.*, vol. 136, no. 19, pp. 6790–6793, 2014.
[225] W. Zhang, Z.-Y. Wu, H.-L. Jiang, and S.-H. Yu, "Nanowire-directed templating synthesis of metal–organic framework nanofibers and their derived porous doped carbon nanofibers for enhanced electrocatalysis," *J. Am. Chem. Soc.*, vol. 136, no. 41, pp. 14,385–14,388, 2014.
[226] H. X. Zhong, J. Wang, Y. W. Zhang, W. L. Xu, W. Xing, D. Xu, Y. F. Zhang, and X. B. Zhang, "ZIF-8 derived graphene-based nitrogen-doped porous carbon sheets as highly efficient and durable oxygen reduction electrocatalysts," *Angew. Chem. Int. Ed.*, vol. 53, pp. 14,235–14,239, 2014.
[227] T. Y. Ma, S. Dai, M. Jaroniec, and S. Z. Qiao, "Metal–organic framework derived hybrid Co3O4-carbon porous nanowire arrays as reversible oxygen evolution electrodes," *J. Am. Chem. Soc.*, vol. 136, no. 39, pp. 13,925–13,931, 2014.
[228] B. Y. Xia, Y. Yan, N. Li, H. B. Wu, X. W. Lou, and X. Wang, "A metal–organic framework-derived bifunctional oxygen electrocatalyst," *Nature Energy*, vol. 1, pp. 15006, 2016.
[229] G. Wu, K. L. More, C. M. Johnston, and P. Zelenay, "High-performance electrocatalysts for oxygen reduction derived from polyaniline, iron, and cobalt," *Science*, vol. 332, no. 6028, pp. 443–447, 2011.
[230] B. Winther-Jensen, O. Winther-Jensen, M. Forsyth, and D. R. MacFarlane, "High rates of oxygen reduction over a vapor phase–polymerized PEDOT electrode," *Science*, vol. 321, no. 5889, pp. 671–674, 2008.
[231] Y. Cui, Z. Wen, X. Liang, Y. Lu, J. Jin, M. Wu, and X. Wu, "A tubular polypyrrole based air electrode with improved O 2 diffusivity for Li–O 2 batteries," *Energy Environ. Sci.*, vol. 5, no. 7, pp. 7893–7897, 2012.
[232] J. Zhang, Z. Zhao, Z. Xia, and L. Dai, "A metal-free bifunctional electrocatalyst for oxygen reduction and oxygen evolution reactions," *Nature Nanotechnol.*, vol. 10, no. 5, pp. 444–452, 2015.
[233] E. Mirzakulova, R. Khatmullin, J. Walpita, T. Corrigan, N. M. Vargas-Barbosa, S. Vyas, S. Oottikkal, S. F. Manzer, C. M. Hadad, and K. D. Glusac, "Electrode-assisted catalytic water oxidation by a flavin derivative," *Nature Chem.*, vol. 4, no. 10, pp. 794–801, 2012.
[234] M. Mirzaeian and P. J. Hall, "Characterizing capacity loss of lithium oxygen batteries by impedance spectroscopy," *J. Power Sources*, vol. 195, no. 19, pp. 6817–6824, 2010.
[235] M. Mirzaeian and P. J. Hall, "Preparation of controlled porosity carbon aerogels for energy storage in rechargeable lithium oxygen batteries," *Electrochim. Acta*, vol. 54, no. 28, pp. 7444–7451, 2009.
[236] C. Tran, X.-Q. Yang, and D. Qu, "Investigation of the gas-diffusion-electrode used as lithium/air cathode in non-aqueous electrolyte and the importance of carbon material porosity," *J. Power Sources*, vol. 195, no. 7, pp. 2057–2063, 2010.
[237] G. O. Shitta-Bey, M. Mirzaeian, and P. J. Hall, "The electrochemical performance of phenol-formaldehyde based activated carbon electrodes for lithium/oxygen batteries," *J. Electrochem. Soc.*, vol. 159, no. 3, pp. A315–A320, 2012.
[238] Y. Zhao, R. Nakamura, K. Kamiya, S. Nakanishi, and K. Hashimoto, "Nitrogen-doped carbon nanomaterials as non-metal electrocatalysts for water oxidation," *Nature Commun.*, vol. 4, pp. 2390–2396, 2013.
[239] S. S. Shinde, C.-H. Lee, A. Sami, D.-H. Kim, S. U. Lee, and J.-H. Lee, "Scalable 3-D carbon nitride sponge as an efficient metal-free bifunctional oxygen electrocatalyst for rechargeable Zn–air batteries," *ACS Nano*, vol. 11, no. 1, pp. 347–357, 2017.
[240] S. Wang, E. Iyyamperumal, A. Roy, Y. Xue, D. Yu, and L. Dai, "Vertically aligned BCN nanotubes as efficient metal-free electrocatalysts for the oxygen reduction reaction: A synergetic effect by co-doping with boron and nitrogen," *Angew. Chem. Int. Ed.*, vol. 50, no. 49, pp. 11,756–11,760, 2011.
[241] K. Gong, F. Du, Z. Xia, M. Durstock, and L. Dai, "Nitrogen-doped carbon nanotube arrays with high electrocatalytic activity for oxygen reduction," *Science*, vol. 323, no. 5915, pp. 760–764, 2009.
[242] X. Bai, E. Wang, J. Yu, and H. Yang, "Blue–violet photoluminescence from large-scale highly aligned boron carbonitride nanofibers," *Appl. Phys. Lett.*, vol. 77, no. 1, pp. 67–69, 2000.
[243] W.-Q. Han, J. Cumings, and A. Zettl, "Pyrolytically grown arrays of highly aligned B x C y N z nanotubes," *Appl. Phys. Lett.*, vol. 78, no. 18, pp. 2769–2771, 2001.
[244] X. Huang, Z. Zeng, Z. Fan, J. Liu, and H. Zhang, "Graphene-based electrodes," *Adv. Mater.*, vol. 24, no. 45, pp. 5979–6004, 2012.
[245] X. Huang, X. Qi, F. Boey, and H. Zhang, "Graphene-based composites," *Chem. Soc. Rev.*, vol. 41, no. 2, pp. 666–686, 2012.
[246] J. Duan, S. Chen, M. Jaroniec, and S. Z. Qiao, "Heteroatom-doped graphene-based materials for energy-relevant electrocatalytic processes," *ACS Catal.*, vol. 5, no. 9, pp. 5207–5234, 2015.
[247] X. H. Li and M. Antonietti, "Polycondensation of boron-and nitrogen-codoped holey graphene monoliths from molecules: Carbocatalysts for selective oxidation," *Angew. Chem. Int. Ed.*, vol. 52, no. 17, pp. 4572–4576, 2013.
[248] J. P. Paraknowitsch and A. Thomas, "Doping carbons beyond nitrogen: an overview of advanced heteroatom doped carbons with boron, sulphur and phosphorus for energy applications," *Energy Environ. Sci.*, vol. 6, no. 10, pp. 2839–2855, 2013.
[249] H. B. Yang, J. Miao, S.-F. Hung, J. Chen, H. B. Tao, X. Wang, L. Zhang, R. Chen, J. Gao, and H. M. Chen, "Identification of catalytic sites for oxygen reduction and oxygen evolution in N-doped graphene materials: Development of highly efficient metal-free bifunctional electrocatalyst," *Sci. Adv.*, vol. 2, no. 4, pp. e1501122, 2016.
[250] H. Wu, H. Li, X. Zhao, Q. Liu, J. Wang, J. Xiao, S. Xie, R. Si, F. Yang, and S. Miao, "Highly doped and exposed Cu (i)–N active sites within graphene towards efficient oxygen reduction for zinc–air batteries," *Energy Environ. Sci.*, vol. 9, no. 12, pp. 3736–3745, 2016.
[251] P. Chen, T. Y. Xiao, Y. H. Qian, S. S. Li, and S. H. Yu, "A nitrogen-doped graphene/carbon nanotube nanocomposite with synergistically enhanced electrochemical activity," *Adv. Mater.*, vol. 25, no. 23, pp. 3192–3196, 2013.
[252] J. Yang, H. Sun, H. Liang, H. Ji, L. Song, C. Gao, and H. Xu, "A highly efficient metal-free oxygen reduction electrocatalyst assembled from carbon nanotubes and graphene," *Adv. Mater.*, vol. 28, no. 23, pp. 4606–4613, 2016.
[253] Z. Lu, H. Wang, D. Kong, K. Yan, P.-C. Hsu, G. Zheng, H. Yao, Z. Liang, X. Sun, and Y. Cui, "Electrochemical tuning of layered lithium transition metal oxides for improvement of oxygen evolution reaction," *Nature Commun.*, vol. 5, 2014.

N